Open access • Journal Article • DOI:10.1021/JP808145X

Effect of cross-linking on the diffusion of water, ions, and small molecules in hydrogels. — Source link

Yanbin Wu, Sony Joseph, Narayana R. Aluru

Institutions: University of Illinois at Urbana–Champaign

Published on: 24 Feb 2009 - Journal of Physical Chemistry B (American Chemical Society)

Topics: Diffusion (business) and Self-healing hydrogels

EFFECT OF CROSS-LINKING ON THE DIFFUSION OF WATER, IONS AND SMALL MOLECULES IN HYDROGELS

BY

YANBIN WU

THESIS

Submitted in partial fulfillment of the requirements
for the degree of Master of Science in Department of Mechanical Science and Engineering
in the Graduate College of the
University of Illinois at Urbana-Champaign, 2011

Urbana, Illinois

Master's Committee:

Professor Narayana R. Aluru, Chair

Abstract

Understanding the diffusion of small molecules in hydrogel system is of major importance in a variety of applications including drug delivery systems, tissue engineering and contact lens. Cross-linking density of hydrogels has been commonly used to tune key parameters like mesh size and molecular weight between cross-linkers, in order to change macroscopic properties of hydrogels. In this thesis, molecular dynamics investigations of chemically-cross-linked poly(ethylene glycol) (PEG) hydrogels are reported with the aim of exploring the diffusion properties of water, ions, and rhodamine within the polymer at the molecular level. The water structure and diffusion properties were studied at various cross-linking densities with molecular weights of the chains ranging from 572 to 3400. As the cross-linking density is increased, the water diffusion decreases and the slowdown in diffusion is more severe at the polymer-water interface. The water diffusion at various cross-linking densities is correlated with the water hydrogen bonding dynamics. The diffusion of ions and rhodamine also decreased as the cross-linking density is increased. The variation of diffusion coefficient with cross-linking density is related to the variation of water content at different cross-linking densities. Comparison of simulation results and obstruction scaling theory for hydrogels showed similar trends.

To Father and Mother.

Acknowledgments

This project would not have been possible without the support of many people. Many thanks to my adviser, Prof. N. R. Aluru, who guided me through my understanding and progress of this project, who read my numerous revisions and helped make sense of the confusion. Thanks to my parents, and numerous friends who endured this long process with me, always offering support and love.

Table of Contents

List of Tables . . . . . **vii**

List of Figures . . . . . **viii**

List of Abbreviations . . . . . **ix**

Chapter 1 Introduction **1**
1.1 Hydrogels 1
1.2 Review of experimental and theoretical studies of hydrogels 1
1.3 Review of molecular dynamics simulation of hydrogels 2
1.4 PEGDA hydrogels 2

Chapter 2 Molecular Dynamics Simulation **4**
2.1 Basics and techniques 4
2.1.1 Periodic boundary conditions 5
2.1.2 Temperature coupling 5
2.1.3 PME 5
2.1.4 LINCS algorithm 6
2.2 Static and dynamic properties from MD simulations 6
2.2.1 Radial distribution function 6
2.2.2 Coordination number 6
2.2.3 Hydrogen bonding 7
2.2.4 Hydrogen bonding dynamics 7
2.2.5 Diffusion coefficient 7

Chapter 3 Methods **8**
3.1 Simulation system setup 8
3.1.1 Cross-linked PEGDA 8
3.1.2 Solvation of PEGDA network 8
3.1.3 Small molecules in PEGDA hydrogel 9
3.2 Force Field 11
3.2.1 Interatomic potential functions 12
3.2.2 United-atom model and all-atom model 14
3.2.3 Force field parameters for PEG 14
3.2.4 Water model 16
3.2.5 Force field parameters for interactions between PEG and water 16
3.2.6 Force field parameters for rhodamine 18
3.2.7 Force field parameters for cross-linker and ions 22
3.2.8 Cross-interaction terms and validation 22
3.3 Simulation details 24
3.3.1 Simulation parameters 24
3.3.2 System equilibration and data collection 24

Chapter 4 Water structure and hydrogen bonding in hydrogel 25
4.1 Radial distribution function between polymer and water 25
4.2 Water hydrogen bonding structure 27
4.3 Hydrogen bond dynamics 27

Chapter 5 Diffusion of molecules in hydrogel 30
5.1 Diffusion of water in hydrogels 30
5.1.1 Residence time of water 30
5.1.2 Diffusion coefficient of water 30
5.2 Diffusion of ions in hydrogels 30
5.3 Diffusion of rhodamine in hydrogels 31
5.4 Comparison with theory 33
5.4.1 Amsden's obstruction scaling theory 33
5.4.2 Comparison between MD results and Amsden's theory 34

Chapter 6 Conclusions 36

References 37

List of Tables

3.1 System composition and equilibrated mesh size. n is the degree of polymerization before cross-linking. Mesh size is a function of n. . . . 9
3.2 Atom numbering for the PEG molecule. . . . 15
3.3 Lennard-Jones parameters for the PEG molecule. . . . 15
3.4 Harmonic bond stretching parameters for the PEG molecule. . . . 15
3.5 Harmonic angle bending parameters for the PEG molecule. . . . 15
3.6 The periodic dihedral function parameters for the PEG molecule. . . . 15
3.7 The Ryckaert-Bellemans dihedral function parameters for the PEG molecule. All the Ci coefficients are in the unit of $kcal/mol$ . . . 16
3.8 Lennard-Jones parameters and partial charges for the SPC/E water molecule. . . . 16
3.9 Lennard-Jones parameters for the PEG-water vdW interactions. The PEG-water hydrogen interaction has zero ϵ value and is not shown in the table. . . . 17
3.10 Atom numbering for the rhodamine molecule. . . . 18
3.11 Lennard-Jones parameters for the rhodamine and cross-linker molecules. . . . 19
3.12 Lennard-Jones parameters for the rhodamine and cross-linker pair interactions. For atom pairs not shown in this table, the pair Lennard-Jones parameters are the same as the the ones in Table 3.11 . . . 19
3.13 Harmonic bond stretching parameters for the rhodamine molecule. . . . 19
3.14 Harmonic angle bending parameters for the rhodamine molecule. . . . 20
3.15 Urey-Bradley angle bending parameters for the rhodamine molecule. . . . 20
3.16 The periodic dihedral function parameters for the rhodamine molecule. . . . 21
3.17 Atom numbering for the cross-linker. . . . 22
3.18 Harmonic bond stretching parameters for the cross-linker. . . . 22
3.19 Harmonic angle bending parameters for the cross-linker. . . . 23
3.20 Urey-Bradley angle bending parameters for the cross-linker. . . . 23
3.21 The periodic dihedral function parameters for the cross-linker. . . . 23
3.22 Lennard-Jones parameters for the the ion molecules. . . . 23

4.1 Average coordination number for different cross-linking densities. . . . 26
4.2 The average number of hydrogen bonds per water molecule in each region for different cross-linking densities. The last column shows water-water hydrogen bonding in region I, not including polymer-water hydrogen bonding. Regions II, III, and IV do not have any polymer-water HB. For region IV, at the highest cross-linking density n=13, there is no bulk region IV. . . . 27
4.3 Number of hydrogen bonds per polymer ether oxygen for different cross-linking densities in region I. . . . 27

5.1 Physical properties of the hydrogel used in Amsden's obstruction scaling theory. . . . 34
5.2 Hydrodynamic radii and modified hydrodynamic radii used in this work for water, ions and rhodamine. . . . 34

List of Figures

3.1 (a) Chemical structure of PEG. (b) Chemical structure of PEGDA. (c) 6 PEGDA chain ends meet and form cyclododecane as cross-linking point. (d) Cross-linked network with 2×2×2 cells in three dimensions. (e) Chemical structure of rhodamine. (f) Visualization of simulation box with polymer network, water, rhodamine and chloride molecules. yellow: carbon, red: oxygen, white: hydrogen. 10
3.2 Equilibrated water content (EWC) used in the simulations for different cross-linking densities. EWC is the volume fraction of water in the simulation box. 11
3.3 Atom numbering for PEG 15
3.4 The radial distribution function of the oxygen of the DME with the oxygen of water in DME-water mixture with the mole fraction of DME as 0.04. Solid line is from this work and circles are from Bedrov et al. 17
3.5 Atom numbering for rhodamine 18
3.6 Atom numbering for cross-linker 22

4.1 Radial distribution function (RDF) between oxygens of polymer ether and oxygen of water and between water oxygens in bulk water. Inset: amplification of the first peak. The RDF, $g_{OP-OW}(r)$, can be computed by normalizing the local density of water molecules at a distance of r from the polymer ether oxygens with the average density of water molecules in the total system. Water is divided into regions I, II, III and IV according to the distance from the polymer. 26
4.2 Decay of autocorrelation function $c(t)$ for polymer-water (P-W) and water-water (W-W) hydrogen bonding in region I. The autocorrelation function for the lowest (n=78) and the highest (n=13) cross-linking density cases are shown. 28
4.3 The relaxation time τ_R from the stretched exponential fit of the water-water HB autocorrelation function in regions I, II, III and IV. 29

5.1 Diffusion of water in different regions as a function of the cross-linking density of the gel. . . 31
5.2 Normalized diffusion of water, ions and rhodamine as a function of cross-linking density obtained using molecular dynamics and theoretical prediction. The diffusion coefficient D_g is normalized with respect to the diffusion coefficient in bulk water D_0. Diffusion of (a) water (b) chloride ion (c) sodium ion and (d) rhodamine. For chloride ion, polymer fiber radius based on MD radial distribution function, r_{fMD}=0.5535 nm, is used, instead of r_f calculated from equation (5.2). 32

List of Abbreviations

DME	dimethoxyethane
LJ	Lennard-Jones
MD	molecular dynamics
PAA	poly(acrylic acid)
PEG	poly(ethylene glycol)
PEGDA	poly(ethylene glycol) diacrylate
POM	poly(oxymethylene)
PVA	poly(vinyl alcohol)
PVME	poly(vinyl methyl ether)
QENS	quasi-elastic neutron scattering
RDF	radial distribution function
vdW	van der Waals

Chapter 1

Introduction

1.1 Hydrogels

Hydrogels, composed of polymer networks and water, have been used increasingly in drug delivery systems, tissue engineering, contact lenses, etc., [1, 2, 3, 4, 5] due to their interesting structural and mechanical properties. The solid-like character of the hydrogel system plays an important role by providing mechanical stability. The hydrogel system also maintains dynamic behavior typical of liquid phases [5]. Two properties of hydrogels, high water content and rubber-like nature, make them akin to a natural tissue. Biocompatibility and cross-linked structure are key properties of hydrogels that allow for various applications.

Cross-linking allows immobilization of active agents and biomolecules and helps drug release at a well defined rate. Cross-linking density is commonly used to tune key parameters like mesh size and molecular weight between cross-linkers, in order to change macroscopic properties such as diffusion and Young's modulus. Among the dynamic properties, diffusion of small molecules, such as nutrients, is essential for vitality of living cells in biological systems.

1.2 Review of experimental and theoretical studies of hydrogels

In order to utilize hydrogels for various applications, it is essential to understand their material properties, flexibility, interactions with solutes and transport phenomena. A cross-linked network is difficult to be analyzed by experimental techniques of chromatography and fractionation owing to the network's inability to dissolve. Deeper insight into dynamic processes occurring within hydrogels have become possible by techniques such as high-flux neutron sources and X-ray synchrotrons [6, 7, 8]. Diffusion in hydrogel has been studied extensively using Quasi-Elastic Neutron Scattering (QENS) [9, 10], Nuclear Magnetic Resonance (NMR) [11, 12, 13], side-by-side diffusion cells [14], fluorescence correlation spectroscopy [15, 16], refractive index method [17], etc.

Many physical models have been developed to model the diffusion of small solutes in hydrogels [18, 19].

Solute behavior in hydrogels has been explained in terms of reduction in hydrogel free volume [20, 21, 22], enhanced hydrodynamic drag on the solute [23, 24], increased path length due to obstruction [25, 26], and a combination of hydrodynamic drag and obstruction effects [27]. The theoretical relations are however limited and rely on fitting parameters that are typically not known. With the rapid development of molecular dynamics simulation techniques, it is now possible to study the structure and dynamics of bio-macromolecular systems in an aqueous environment considering explicit water, ion and solute molecules [28, 29].

1.3 Review of molecular dynamics simulation of hydrogels

In recent times, molecular dynamics simulation has been used to study physical gels [30], poly(vinyl alcohol) [31, 10], poly(vinyl methyl ether) [32], poly(N-isopropylacrylamide) [32], polyacrylamide [33], epoxy-amine networks [34], etc. Structure and dynamics of the polymer-water interface in poly(vinyl alcohol) (PVA) for a mesh size of 1 nm was studied recently [10]. Solvent diffusion coefficient and residence times in hydrophilic systems indicate that water behaves as a supercooled liquid phase [10]. Structural and mechanical properties and diffusion of glucose and vitamin D in poly(ethylene glycol) (PEG) and poly (acrylic acid) (PAA) and their double network was investigated by Jang et al. [35]. Effects of confined water in cages of different chemical and structural features, have also been investigated previously in other natural and man-made structures such as vycor glass [36], carbon nanotubes [37, 38], boron-nitride nanotubes [39], zeolites [40], cellular membrane channels [41], proteins [29], carbohydrate solution [42], etc.

1.4 PEGDA hydrogels

Poly (ethylene glycol) (PEG)-based hydrogel network has been increasingly utilized in tissue engineering applications in recent years. This is mainly due to their hydrophilicity and resistance to protein adsorption and biocompatibility. They can also be customized by modifying the chain length and adding biological functional groups. Besides, PEG hydrogel is a promising membrane material for selective removal of CO_2 from a mixture containing light gases such as CH_4, N_2 and H_2 [43].

PEG can be easily cross-linked using acrylate group as a cross-linker. In conventional polymerization, the cross-linking density, defined as the number of cross-linkers divided by the number of monomers, need not be homogeneous throughout the network, but in poly(ethylene glycol) diacrylate (PEGDA) it is homogeneous because the molecular weight between the cross-linkers is the same as that of the PEG monomer. This enables PEGDA to be used as an ideal material for studying gel properties.

Since cross-linking has a significant impact on the structural and dynamic properties of the hydrogel,

we investigate the structural and dynamic properties of a hydrogel consisting of cross-linked PEGDA, water and small solutes (ions and rhodamine) using molecular dynamics (MD) simulations, as they can provide a useful description of water and solute mobility by considering explicit water and partial charge for PEG atoms. Rhodamine is commonly used as a tracer dye in experiments within hydrogel networks to determine the transport properties of the network. Studying rhodamine diffusion also helps to understand the diffusion of similar sized biomolecules in PEGDA.

The rest of the thesis is organized as follows: a brief overview of molecular dynamics simulation techniques and analysis methods is given in Chapter 2. Chapter 3 presents the system setup with the force field used and a description of the construction of the cross-linked structure. In Chapter 4, we investigate the water structure and hydrogen bonding in various regions divided according to the distance from the polymer. Next, in Chapter 5, we present the results and discussion on variation of diffusion coefficients on water, ions, and rhodamine as a function of the cross-linking density. Then the varation of the diffusion coefficients from MD simulations are compared with the prediction from Amsden obstruction scaling theory.

Chapter 2

Molecular Dynamics Simulation

2.1 Basics and techniques

Molecular dynamics simulation represent a system by N interaction particles[44]. At any time, the state of the system is given by (r_i, v_i), where r_i and v_i are the position and velocity of particle i in the system. The motion of the N particles is governed by Newton's law:

$$m_i \frac{\partial^2 r_i}{\partial t^2} = F_i, i = 1 \dots N. \tag{2.1}$$

where m_i is the mass of the particle i, F_i is the force acting on particle i and given by the negative derivative of a potential function $V(r_1, r_2, \dots, r_N)$:

$$F_i = -\frac{\partial V}{\partial r_i} \tag{2.2}$$

More details about the inter-particle potential can be found in the next chapter. The Newton's equation of motion is integrated over the given time interval Δt using leap-frog algorithm to obtain the new velocity and position of particles in the system:

$$v_i(t + \frac{\Delta t}{2}) = v_i(t - \frac{\Delta t}{2}) + \frac{F_i(t)}{m}\Delta t \tag{2.3}$$

$$r_i(t + \Delta t) = r_i(t) + v(t + \frac{\Delta t}{2})\Delta t \tag{2.4}$$

$$\tag{2.5}$$

Δt is optimized for both speed and accuracy of the simulation. Observables of interests like radial distribution and diffusion coefficient can be obtained by analyzing the trajectory after the system has achieved an equilibrium state.

2.1.1 Periodic boundary conditions

The typical length scale and time scale of the system that MD is capable of simulating is a few nanometers and a few nanoseconds. In order to obtain macroscopic properties from MD simulations, periodic boundary conditions are applied. This means that the simulation cell is surrounded by the translation copy of itself. The periodic boundary condition also minimizes the edge effects.

2.1.2 Temperature coupling

The temperature of the simulation system is maintained by the Nosè-Hoover thermostat [45, 46]. For the Nosè-Hoover algorithm, the system Hamitonian is extended by introducing a thermal reservoir and a friction term in the equation of motion. The friction force is proportional to the particle's velocity and a friction parameter ξ. The extended Hamitonian is represented by:

$$\frac{\partial^2 r_i}{\partial t^2} = \frac{F_i}{m_i} - \xi \frac{\partial r_i}{\partial t} \tag{2.6}$$

The equation of motion for the heat bath parameter ξ is given by

$$\frac{d\xi}{dt} = \frac{1}{Q}(T - T_0) \tag{2.7}$$

where T_0 is reference temperature and T is the instantaneous temperature of the system. The constant Q determines the strength of the temperature coupling with the reservoir. Q is computed by

$$Q = \frac{\tau_T^2 T_0}{4\pi^2} \tag{2.8}$$

where τ_T is the period of the oscillation of kinetic energy between the system and reservoir and specified as the simulation input.

2.1.3 PME

Unlike van der Waals interaction, the electrostatic interaction is long-ranged. The calculation of the electrostatic interactions is the most time-consuming step in the MD simulations. Efficient methods such as particle mesh Ewald (PME) method [47, 48] have been developed. In the PME scheme, instead of directly summing wave vectors, the charges are assigned to a grid using cardinal B-spline interpolation. The grid is then Fourier transformed with a three-dimensional FFT algorithm and the reciprocal energy term is obtained by a single sum over the grid in k-space. The electrostatic energy of charges in a three dimensionally

periodic system by PME is given by:

$$V_{coul} = \frac{1}{2V}\sum_{k\neq 0}\frac{4\pi}{k^2}|\rho(k)|^2 exp(-k^2/4\alpha) - (\alpha/\pi)^{1/2}\sum_{i=1}^{N} q_i^2 + \frac{1}{2}\sum_{i\neq j} N\frac{q_i q_j erfc(\alpha^{1/2} r_{ij})}{r_{ij}} \tag{2.9}$$

where V is the volume of the simulation box, k is the reciprocal space vector, q_i is the charge on atom i, $\rho(k) = \sum_{i=1}^{N} q_i exp(ik \cdot r_i)$ and α is the parameter that defines the Gaussian width. The first term is the Fourier sum. The second term is the correction to the self interaction energy between a charge and its periodic image. The third term is the real-space summation term. The PME algorithm scales as $Nlog(N)$.

2.1.4 LINCS algorithm

LINCS is an algorithm that resets the bonds to the correct length after an unconstrained update [49]. LINCS is stable and can only be used with bond constraints and isolated angle constraints. LINCS is used to constrain the internal geometry of the water molecule in the current study.

2.2 Static and dynamic properties from MD simulations

2.2.1 Radial distribution function

The radial distribution function (RDF) $g_{A-B}(r)$ gives the probability density of finding particle B at a distance r from a particle A, averaged over the whole equilibrated trajectory:

$$g_{A-B}(r) = \frac{n_B}{4\pi r^2 dr} / \left(\frac{N_B}{V}\right) \tag{2.10}$$

where n_B is the number of B particles located at the distance r in a sheel of thickness dr from A particles, N_B is the number of B particles in the system and V is the total volume of the system.

2.2.2 Coordination number

The number of atoms A per atom B, or the average coordination number, n_{A-B}, can be evaluated by the following equation:

$$n_{A-B} = \frac{N_B}{V_{box}}\int_0^{R_{min}} 4\pi r^2 g_{A-B}(r) dr \tag{2.11}$$

where N_B is the total number of atoms B in the box, V_{box} is the volume of the box and R_{min} is the position of the first valley.

2.2.3 Hydrogen bonding

The hydrogen bonding (HB) structure between water molecules and that between polar molecules can be studied by analyzing the trajectory. Hydrogen bonding is defined by adopting the geometric criteria where the acceptor-donor (O $\cdots$ O) distance is less than 0.35 nm and the angle (O-H $\cdots$ O) is less than 30^o.

2.2.4 Hydrogen bonding dynamics

The intermittent time autocorrelation function $c(t)$ expresses the probability that a randomly chosen pair of molecules is bonded at time t, provided that a bond existed at time $t = 0$, regardless of whether it was bonded in the interim time. $c(t)$ provides valuable insight into the relaxation of the system's H-bonding network. $c(t)$ is given by

$$c(t) = \frac{\langle h(t)h(0)\rangle}{\langle h(0)h(0)\rangle} \tag{2.12}$$

where $h(t)$ is 1 if molecules are bonded at time t and 0 if not. $\langle\rangle$ denotes average over all pairs of HB at $t = 0$ and over many time steps.

2.2.5 Diffusion coefficient

The diffusion coefficient is obtained from the long-time slope of the mean square displacement:

$$D = \frac{1}{6}\lim_{t\to\infty}\frac{d}{dt}\langle|\mathbf{r}(t) - \mathbf{r}(0)|^2\rangle \tag{2.13}$$

where $\mathbf{r}(t)$ and $\mathbf{r}(0)$ are the position vectors of the center of mass at time t and 0, respectively, with an average performed over the simulation time and over all the number of molecules.

Chapter 3

Methods

3.1 Simulation system setup

3.1.1 Cross-linked PEGDA

For our simulations we used a cross-linked PEGDA structure with an ideal network without any free dangling ends or self-looping or entanglements. Figure 3.1(a) shows a PEG chain with n monomers. Each PEGDA molecule (see Figure 3.1(b)) is a PEG chain connected to acrylate groups at both ends that serve as cross-linkers. Under the influence of ultra-violet rays, the acrylate double bond breaks and connects with other PEG chains (see Figure 3.1(c)) to form the cross-linking point. We used an ideally cross-linked unit cell where six PEGDA chains meet at the cross-linking point, forming a cyclododecane ring structure at the unit cell center (see Figure 3.1(c) and Figure 3.1(d)), similar to the approach presented by Jang et al. [35].

The cross-linking density is defined as the number of cross-linkers (acrylate groups at the ends) divided by the number of monomers (ethylene glycol). For ideal cross-linking, the cross-linking density is $1/n$, where n is the degree of polymerization of the PEG chain. Higher the degree of polymerization of the PEG chain, the lower is the cross-linking density. The ideally cross-linked unit cell was periodically replicated along xyz-directions, forming a 3-D hydrogel simulation box, as shown in Figure 3.1(d). We systematically built gels with different cross-linking densities and investigated diffusion of water and small solutes in these gels. Table 3.1 shows the different cross-linking density cases we considered.

3.1.2 Solvation of PEGDA network

The cross-linked PEGDA structures were then solvated by water. We chose the number of water molecules to insert into the system based on experimental measurements. Using results of Padmavathi et al. [50], which gives the equilibrium water content for a wide range of cross-linking densities, we calculated the number of water molecules to insert into the system. The swelling ratios in experiments were for a pre-polymer PEG solution of around 30% w/w concentration. The equilibrated water content (EWC) used in our system is

Table 3.1: System composition and equilibrated mesh size. n is the degree of polymerization before cross-linking. Mesh size is a function of n.

pre-polymer	PEG572	PEG1000	PEG1500	PEG2000	PEG3400
n	13	23	34	45	78
cross-linking density$(1/n)$%	7.69	4.35	2.94	2.22	1.28
equilibrated water content/%	74.7	84.2	85.5	89.9	90.9
polymer volume content/%	25.3	15.8	14.5	10.1	9.1
mesh size/nm	2.28	3.14	3.64	4.47	5.49
number of water molecules per cell	291	855	1353	2636	4984
number of cells	$2 \times 2 \times 2$	$2 \times 2 \times 2$	$2 \times 2 \times 2$	$1 \times 1 \times 1$	$1 \times 1 \times 1$
simulation box size/nm	4.56	6.28	7.28	4.47	5.49

given in Table 3.1. EWC is defined as the ratio of the volume of water in the simulation box to the total volume of the simulation box. Figure 3.2 depicts the EWC data in graphical form. We also compared the water content we used against several other papers [51, 52, 53, 54, 11] that had some of the cross-linking densities we considered, and found our numbers to be reasonable.

3.1.3 Small molecules in PEGDA hydrogel

For the case with ions, we assumed that the number of water molecules remained the same even after adding ions such that there was essentially no swelling after we inserted ions into the system. The NaCl ion concentration considered was 0.5 M within the gel.

For the rhodamine case, we had to consider the fact that if the concentration of rhodamine was above 10^{-6} M, typically rhodamine aggregation occurred by stacking up on its 3-ring xanthylium plane (rhodamine structure is shown in Figure 3.1(e)) and this hindered fluorescent yield and diffusion. In experiments, to avoid aggregation a very dilute solution is used, but in simulations, such low concentrations would need an extremely large box size and would be computationally expensive. So in our simulations, we used only one rhodamine in the system with the simulation box size ranging from 4.56 nm to 7.28 nm, which is much larger than 4 Å, the distance between the planes of rhodamine molecules in a dimer structure formed during aggregation [55].

The final system composition and equilibrated mesh size for the different cases are summarized in Table 3.1. Figure 3.1(f) shows a snapshot of the simulation box comprising of the polymer network, water, rhodamine, and chloride ions.

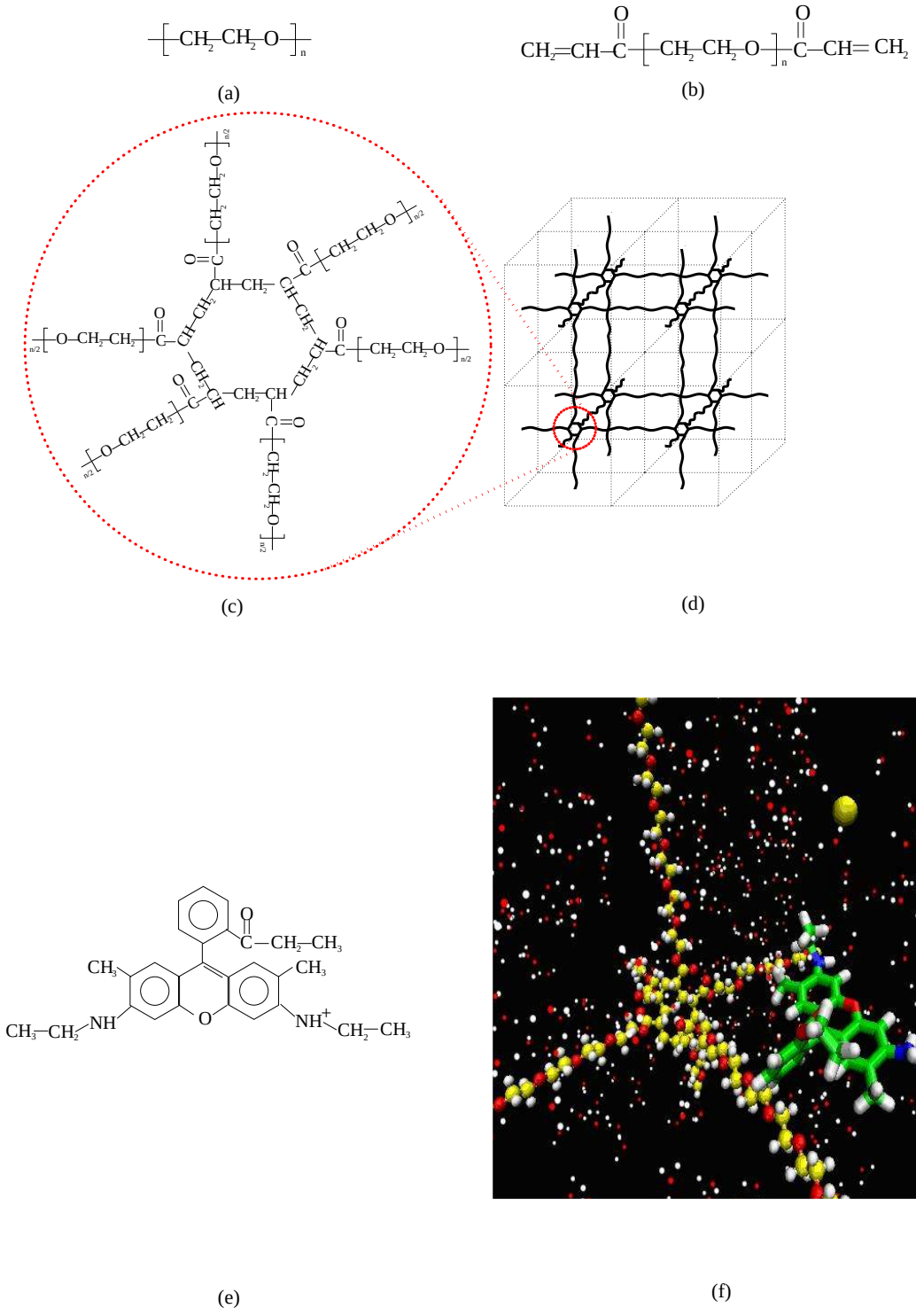

Figure 3.1: (a) Chemical structure of PEG. (b) Chemical structure of PEGDA. (c) 6 PEGDA chain ends meet and form cyclododecane as cross-linking point. (d) Cross-linked network with 2×2×2 cells in three dimensions. (e) Chemical structure of rhodamine. (f) Visualization of simulation box with polymer network, water, rhodamine and chloride molecules. yellow: carbon, red: oxygen, white: hydrogen.

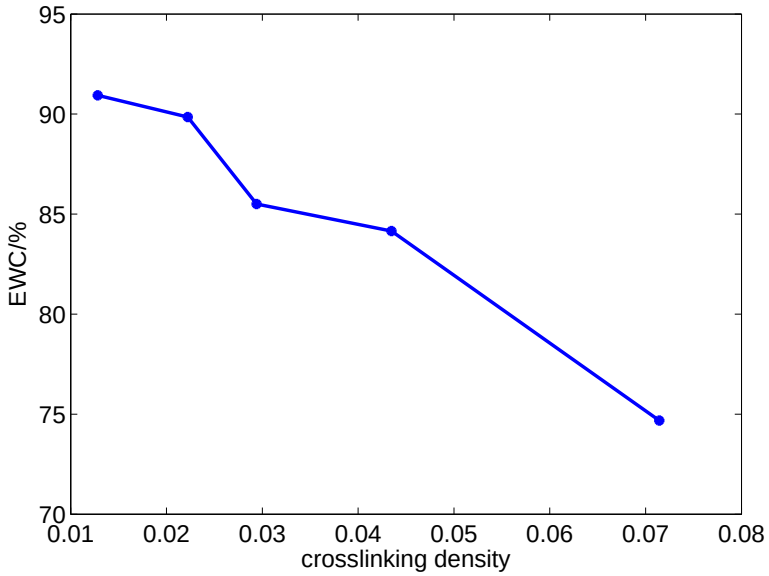

Figure 3.2: Equilibrated water content (EWC) used in the simulations for different cross-linking densities. EWC is the volume fraction of water in the simulation box.

3.2 Force Field

In general, current force fields in literature can be divided into three categories: (a) the force field parameters are developed based on a broad training set of molecules such as small organic molecules, peptides, or amino acides. This category includes AMBER[56, 57, 58], COMPASS[59], OPLS-AA[60] and CHARMM[61]; (b) generic potentials such as DREIDING[62] and UFF[63] that are not parameterized to reproduce properties of any particular set of molecules but based on simple hybridization considerations; (c) specialized force fields that are parameterized to reproduce properties of a specific compound that cannot be properly represented by existing force field sets.

Two major issues must be considered for the choice of a proper potential: the quality of the potential and the transferability of the potential. The quality of a potential can be evaluated by the quality and quantity of data used to parameterize the potential. The issue of transferability of a potential is encountered when a high-quality force field, which is adequatedly validated by a set of training molecules, is used to describe a compound not in the training set[64].

Properties of predicted properties using molecular dynamics simulations depend on the accuracy of the force fields. In the current study, PEG is a polar molecule and special care should be taken for the PEG-oxygen and water hydrogen bonding interaction. Specialized force field was used for PEG and PEG-water interaction. For other molecules, slightly modified CHARMM force field was used.

3.2.1 Interatomic potential functions

The interatomic potential energy is partitioned as follows:

$$E_{total} = E_{vdW} + E_Q + E_{bond} + E_{angle} + E_{dihedral} \tag{3.1}$$

where E_{total}, E_{vdW}, E_Q, E_{bond}, E_{angle}, and $E_{dihedral}$ are the total, van der Waals (vdW), electrostatic, bond stretching, angle bending, and torsion energies, respectively.

The vdW interaction is represented by Lennard-Jones(LJ) potential. The LJ potential is pairwise and additive. The LJ potential form between atom i and atom j is:

$$E_{LJ}(r_{ij}) = 4\epsilon_{ij}\left[\left(\frac{\sigma_{ij}}{r_{ij}}\right)^{12} - \left(\frac{\sigma_{ij}}{r_{ij}}\right)^{6}\right] \tag{3.2}$$

where ϵ_{ij} is the depth of the potential well and σ_{ij} is the separation distance where the LJ interaction between atom i and atom j is zero.

The vdW interaction can also be represented by Buckingham potential with the formula as follows:

$$E_{BK}(r_{ij}) = Aexp(-rB) - Cr^{-6} = \frac{D_v}{\xi - 6}\left[6e^{\xi(1-\frac{Rv}{r_{ij}})} - \xi\left(\frac{R_v}{r_{ij}}\right)^{6}\right] \tag{3.3}$$

where Dv is the depth of the potential well corresponding to ϵ in LJ formula and Rv is the position of the potential well corresponding to $2^{1/6}\sigma$. The Buckingham potential parameters are usually given in the form of (A, B, C). The transformations from (A, B, C) in Buckingham formula to (ϵ, σ) in LJ formula to reproduce the same position and depth of the potential well are given by:

$$R_v = -\frac{7}{B}W\left(-\frac{B}{7}\left(\frac{6C}{AB}\right)^{\frac{1}{7}}\right) \tag{3.4}$$

$$\xi = BR_v \tag{3.5}$$

$$D_v = \frac{A(\xi - 6)}{6e^{\xi}} \tag{3.6}$$

$$\sigma = (\frac{1}{2})^{1/6}R_v \tag{3.7}$$

$$\epsilon = D_v \tag{3.8}$$

where W is Lambert W function. Note that Lambert W function is double-valued for $Y \in (-1/e, 0)$. The matlab built-in Lambert W function can be called by lambertw(-1, Y).

The electrostatic interaction is given by Coulomb potential:

$$E_Q(r_{ij}) = f\frac{q_i q_j}{r_{ij}} \tag{3.9}$$

where q_i and q_j are the partial charge on atom i and atom j, and f is the electric conversion factor defined by $f = \frac{1}{4\pi\epsilon_0} = 138.935kJ\,mol^{-1}\,nm\,e^{-2}$.

The vdW and electrostatic interactions are applied to atom pairs in different molecules, or atom pairs separated by more than two bonds within the same molecule. The atom pairs separated by three bonds could be represented by different vdW parameters (ϵ^p, σ^p).

The bond stretching between two covalently bonded atom i and atom j is represented by a harmonic potential

$$E_{bond}(r_{ij}) = k^b_{ij}(r_{ij} - b_{ij})^2 \tag{3.10}$$

where k^b_{ij} is the bond stretching constant and b_{ij} is the equilibrium bond length.

The angle bending between three neighboring atoms i-j-k can be represented by a harmonic potential or the Urey-Bradley potential on the angle θ_{ijk}. The harmonic potential has a mathematical formula of

$$E_{angle}(\theta_{ijk}) = k^\theta_{ijk}(\theta_{ijk} - \theta^0_{ijk})^2 \tag{3.11}$$

where k^θ_{ijk} is the angle bending constant and θ^0_{ijk} is the equilibrium angle. The bond Urey-Bradley angle vibration between atoms i-j-k is represented by a harmonic potential on the angle θ_{ijk} plus a harmonic correction on the distance between the atoms i and k. This potential is mainly used in the CHARMM force field [61]. The function form is given by

$$E_{angle}(\theta_{ijk}) = k^\theta_{ijk}(\theta_{ijk} - \theta^0_{ijk})^2 + k^{UB}_{ijk}(r_{ik} - r^0_{ik}) \tag{3.12}$$

The dihedral interaction can be either represented by the GROMOS periodic function or the Ryckaert-Bellemans potential. The periodic function is given by

$$E_{dih}(\phi_{ijkl}) = k_\phi(1 + cos(n\phi - \phi_s)) \tag{3.13}$$

where ϕ is defined according to IUPAC/IUB convention as the angle between the ijk and jkl planes, with zero corresponding to the cis configuration (i and l on the same side). The Ryckaert-Bellemans potential

has the following formula

$$E_{dih}(\phi_{ijkl}) = \sum_{n=0}^{5} C_n (cos\psi)^n \tag{3.14}$$

where $\psi = \phi - 180°$.

3.2.2 United-atom model and all-atom model

In the all-atom model, each atom in the molecule is treated explicitly. In the united-atom model, hydrogen atoms are not treated explicitly in the simulation of hydrocarbon chains but combined into the carbon atoms they are bounded to. This treatment of hydrogen atoms removes the highest frequency oscillations (i.e. the C-H bond stretching, H-C-H and H-C-C angle bending) from the model thus a bigger time step can be used. Also the total number of atoms in the simulation box is decreased due to the implicit representation of hydrogen atoms. So the united-atom model can speed up the simulation, compared to the all-atom model. But the united-atom model is only feasible for the study of the structure and relaxation properties without any local specific interactions (strong electrostatic interactions, hydrogen bonding, etc.)[64]. For the system we are interested, PEG is a polar molecule and cannot be represented propertly by united-atom model. So all atoms in the PEG molecules are treated explicitly. For consistency, all atoms in other molecules are treated explicitly as well.

3.2.3 Force field parameters for PEG

The force field parameters for the PEG chain follow Smith et al. [65]. The parameters for the non-bonded dispersion and repulsion interactions were adopted from an empirical force field which successfully described the crystal structures and energetics of poly(oxymethylene) (POM) [66], where the OP-OP function parameters were specially obtained by fitting to experimental lattice parameters and lattice energies of POM. The energies and geometries dimethoxyethane conformer and rotational barriers between the lowest energy conformer from electronic structure methods were used to parameterize the bonded interaction. The force field was validated by comparing the radial distribution function of gas-phase DME to the electron diffraction experiments[65]. The atom numbering, LJ parameters, harmonic bond stretching parameters, harmonic angle bending parameters, periodic dihedral function parameters and the Ryckaert-Bellemans dihedral function parameters are shown in Table 3.2, 3.3, 3.4, 3.5, 3.6 and 3.7.

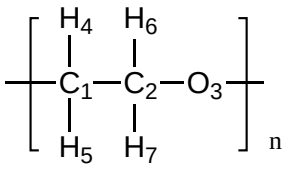

Figure 3.3: Atom numbering for PEG

Table 3.2: Atom numbering for the PEG molecule.

Number	Atom type	Charge
C1, C2	CP	-0.066
O3	OP	-0.256
H4-H7	HP	0.097

Table 3.3: Lennard-Jones parameters for the PEG molecule.

Atom types	$\epsilon(kcal/mol)$	$\sigma(\mathring{A})$
CP-CP	0.0948	3.4494
HP-HP	0.0098	3.0022
OP-OP	0.1991	2.8500
CP-OP	0.1526	3.0795
CP-HP	0.0520	2.9169
OP-HP	0.0447	2.9202

Table 3.4: Harmonic bond stretching parameters for the PEG molecule.

Atom types	$k^b_{ij}(kcal/mol/\mathring{A}^2)$	$b_{ij}(\mathring{A})$
CP-CP	309.0	1.51
CP-HP	327.5	1.09
OP-CP	369.5	1.39

Table 3.5: Harmonic angle bending parameters for the PEG molecule.

Atom types	$k^\theta_{ijk}(kcal/mol/rad^2)$	$\theta^0_{ijk}(^\circ)$
CP-CP-CP	53.5	111.0
CP-CP-HP	43.0	109.5
HP-CP-HP	38.5	108.3
CP-CP-OP	86.0	109.0
OP-CP-HP	56.0	110.1
CP-OP-CP	74.5	111.6

Table 3.6: The periodic dihedral function parameters for the PEG molecule.

Atom types	n	$k_\phi(kcal/mol)$	$\phi_s(^\circ)$
OP-CP-CP-HP	3	0.28	0.0
CP-CP-CP-HP	3	0.28	0.0
HP-CP-CP-HP	3	0.28	0.0
CP-OP-CP-HP	3	0.81	0.0

Table 3.7: The Ryckaert-Bellemans dihedral function parameters for the PEG molecule. All the Ci coefficients are in the unit of $kcal/mol$

Atom types	$C0$	$C1$	$C2$	$C3$	$C4$	$C5$
OP-CP-CP-OP	0.0000	0.1046	10.6692	0.0000	0.0000	0.0000
CP-OP-CP-CP	0.0000	-0.0837	2.9288	-2.6778	0.0000	0.0000

Table 3.8: Lennard-Jones parameters and partial charges for the SPC/E water molecule.

Atom types	$\epsilon(kcal/mol)$	$\sigma(\mathring{A})$	Charges
OW-OW	0.1554	3.1656	-0.8476
HW-HW	0.0000	0.0000	0.4238

3.2.4 Water model

We used the Single Point Charge/Extended (SPC/E) model [67] for water because this model predicts the experimental water self-diffusion coefficient and dielectric constant pretty well. The SPC/E model is a rigid water model. The oxygen-hydrogen bond length is 1.0 $\mathring{A}$ and the hydrogen-hydrogen distance is 1.633 $\mathring{A}$. This corresponds to an H-O-H angle of 109.47°. The water geometry is maintained by LINCS constraints [49] during the simulation. The partial charges are distributed at the cites of oxygen and hydrogen atoms to reproduce the dipole moment of the water monomer. The LJ interaction parameters are only non-zero for oxygen, making the vdW interaction independent of the water orientation. The LJ parameters and partial changes of the water molecule are shown in Table 3.8.

3.2.5 Force field parameters for interactions between PEG and water

LJ interaction parameters between PEG and water are taken from Bedrov et al. [68], as shown in Table 3.9. The LJ interactions were parameterized by the MP2 level quantum chemistry binding energies of DME/water dimer. A series of dimer binding energies were computed at various separation distance between the DME and water. The electrostatic interaction energy components were subtracted from the total binding energies by the Coulomb potential using the partial changes on PEG and water molecules shown in Table 3.2 and 3.8. The remaining binding energy components were fitted to the LJ potential using least square fitting method to obtain the LJ parameters[69, 70, 68]. In order to verify the interaction parameters between PEG and water, we simulated a system composed only of DME chains and water (the mole fraction of DME is 0.04) and calculated the radial distribution function of the oxygen of the DME with the oxygen of water and obtained good agreement with the results of Borodin et al. [68], as shown in Figure 3.4.

Table 3.9: Lennard-Jones parameters for the PEG-water vdW interactions. The PEG-water hydrogen interaction has zero ϵ value and is not shown in the table.

Atom types	$\epsilon(kcal/mol)$	$\sigma(\AA)$
CP-OW	0.2066	3.2817
OP-OW	0.2998	2.9842
HP-OW	0.0663	3.0625

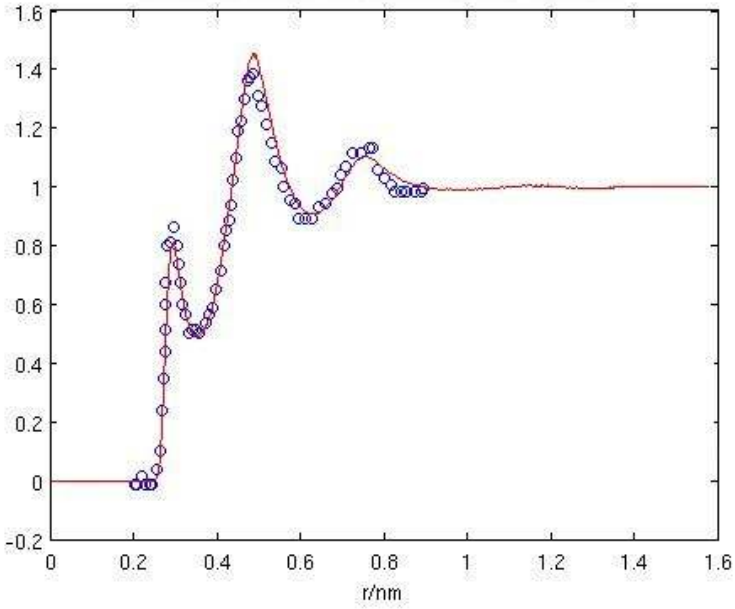

Figure 3.4: The radial distribution function of the oxygen of the DME with the oxygen of water in DME-water mixture with the mole fraction of DME as 0.04. Solid line is from this work and circles are from Bedrov et al.

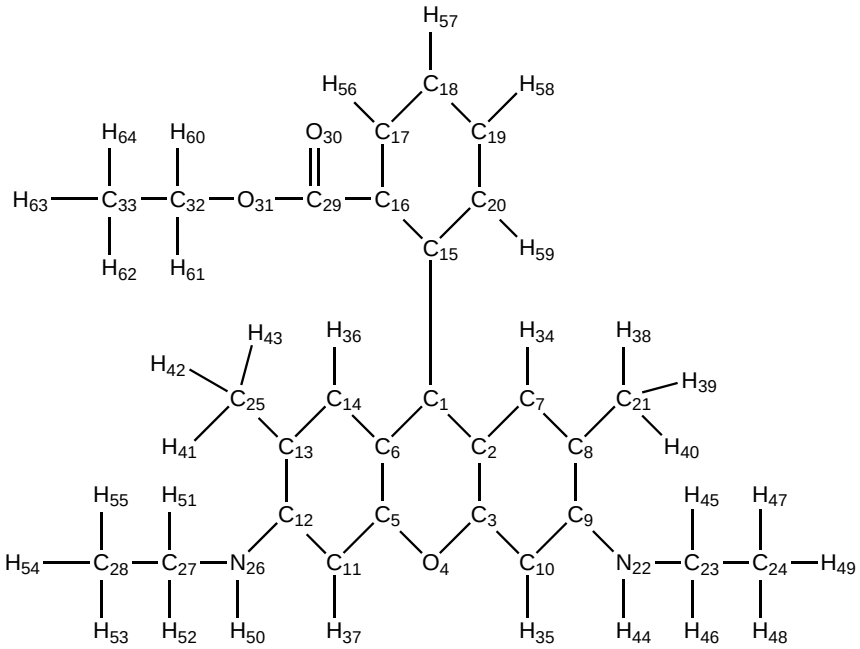

Figure 3.5: Atom numbering for rhodamine

3.2.6 Force field parameters for rhodamine

The force field parameters for rhodamine are from Vaiana et al.[71] and are summarized in Table 3.10, 3.11, 3.13, 3.14, 3.15 and 3.16. This force field is based on CHARMM[61] and refined to the vibrational frequencies and eigenvector projections from quantum chemistry calculations. The derived force field reproduced the experimental crystal structure of rhodamine well.

Table 3.10: Atom numbering for the rhodamine molecule.

Number	Atom type	Charge	Number	Atom type	Charge
C1,C15	CA1R	0.00	C21,C24,C25,C28	CT3R	-0.27
C2,C6,C8,C13,C16	CAR	0.00	C29	CR	0.73
C3,C5	CAR	0.17	O30	OBR	-0.52
O4,O31	OSR	-0.34	C32	CT2R	-0.05
C7,C10,C11	CAR	-0.115	C33	CT3R	-0.27
C14,C17-C20	CAR	-0.115	H34-H37,H56-H59	HPR	0.115
C9,C12	CAR	0.64	H44,H50	HR	0.46
N22,N26	NC2R	-0.60	H38-H43,H45-H49	HAR	0.09
C23,C27	CT2R	-0.18	H51-H55,H60-H64	HAR	0.09

Table 3.11: Lennard-Jones parameters for the rhodamine and cross-linker molecules.

Atom types	$\epsilon(kcal/mol)$	$\sigma(\mathring{A})$
CAR-CAR	0.0700	3.5501
CA1R-CA1R	0.0700	3.5501
CT1R-CT1R	0.0200	4.0536
CT2R-CT2R	0.0550	3.8754
CT3R-CT3R	0.0801	3.6705
CDR-CDR	0.0700	3.5636
OSR-OSR	0.1522	3.1538
OBR-OBR	0.1201	3.0291
NC2R-NC2R	0.2001	3.2963
HPR-HPR	0.0300	2.4200
HCR-HCR	0.0460	0.4000
HAR-HAR	0.0220	2.3520

Table 3.12: Lennard-Jones parameters for the rhodamine and cross-linker pair interactions. For atom pairs not shown in this table, the pair Lennard-Jones parameters are the same as the the ones in Table 3.11

Atom types	$\epsilon^p(kcal/mol)$	$\sigma^p(\mathring{A})$
CT1R-CT1R	0.0100	0.33854
CT2R-CT2R	0.0100	0.33854
CT3R-CT3R	0.0100	0.33854
OBR-OBR	0.1201	0.24945

Table 3.13: Harmonic bond stretching parameters for the rhodamine molecule.

Atom types	$k_{ij}^b(kcal/mol/\mathring{A}^2)$	$b_{ij}(\mathring{A})$
CA1R-CA1R	221.0	1.490
CA1R-CAR	305.0	1.375
CAR-CAR	305.0	1.375
CAR-OSR	300.0	1.335
CAR-CDR	302.0	1.480
CAR-HPR	340.0	1.080
CAR-CT3R	230.0	1.490
CAR-NC2R	463.0	1.365
CT2R-OSR	340.0	1.430
CT2R-CT3R	222.5	1.528
CT2R-HAR	309.0	1.111
CT2R-NC2R	261.0	1.490
CT3R-HAR	322.0	1.111
OSR-CDR	150.0	1.334
CDR-OBR	750.0	1.220
NC2R-HCR	455.0	1.000

Table 3.14: Harmonic angle bending parameters for the rhodamine molecule.

Atom types	$k^{\theta}_{ijk}(kcal/mol/rad^2)$	$\theta^0_{ijk}(^\circ)$
CAR-OSR-CAR	52.5	121.6
CAR-CAR-NC2R	39.4	120.0
OSR-CAR-CAR	76.3	119.0
CAR-NC2R-HCR	39.0	113.4
CAR-NC2R-CT2R	53.0	129.9
CAR-CDR-OBR	37.1	123.0
CAR-CDR-OSR	38.5	113.0
CAR-CAR-CT3R	45.8	122.3
CAR-CT3R-HAR	49.3	107.5
NC2R-CT2R-CT3R	69.1	107.5
HCR-NC2R-CT2R	40.4	120.0
NC2R-CT2R-HAR	51.5	107.5
OSR-CT2R-CT3R	30.9	107.5
HAR-CT2R-OSR	60.0	109.5

Table 3.15: Urey-Bradley angle bending parameters for the rhodamine molecule.

Atom types	$k^{\theta}_{ijk}(kcal/mol/rad^2)$	$\theta^0_{ijk}(^\circ)$	$k^b_{ij}(kcal/mol/\mathring{A}^2)$	$b_{ij}(\mathring{A})$
CAR-CAR-CA1R	40.0	120.0	35.00	2.4162
CAR-CA1R-CAR	40.0	120.0	35.00	2.4162
HPR-CAR-CA1R	30.0	120.0	22.00	2.1525
CA1R-CAR-CDR	89.6	119.5	33.50	2.4162
CAR-CAR-CDR	89.6	119.5	33.50	2.4162
CAR-CAR-HPR	30.0	120.0	22.00	2.1525
CAR-CAR-CAR	40.0	120.0	35.00	2.4162
CT2R-OSR-CDR	40.0	109.6	30.00	2.2651
OSR-CDR-OBR	90.0	125.9	160.00	2.2576
HAR-CT3R-HAR	35.5	108.4	5.40	1.8020
HAR-CT3R-CT2R	34.6	110.1	22.53	2.1790
CT3R-CT2R-HAR	34.6	110.1	22.53	2.1790
HAR-CT2R-HAR	35.5	109.0	5.40	1.8020

Table 3.16: The periodic dihedral function parameters for the rhodamine molecule.

Atom types	n	$k_\phi(kcal/mol)$	$\phi_s(^\circ)$
CA-CA-CA-CA1	2	3.10	180.0
CA-CA-CA1-CA	2	3.10	180.0
CA1-CA-CA-HP	2	4.20	180.0
CA-CA1-CA-HP	2	4.20	180.0
OS-CA-CA-CA1	2	3.10	180.0
CA-CA1-CA-CD	2	4.20	180.0
CA1-CA1-CA-CD	2	4.20	180.0
CA-CA-CA1-CA1	2	2.10	180.0
CA1-CA1-CA-HP	2	3.20	180.0
CA1-CA-CD-OB	2	1.00	180.0
CA1-CA-CD-OS	2	1.00	180.0
CA-CA1-CA1-CA	2	-0.60	0.0
CA-CA1-CA1-CA	4	0.10	0.0
CA-CA-CA-CA	2	3.10	180.0
CA-CA-CA-HP	2	4.20	180.0
OS-CA-CA-CA	2	1.70	180.0
CA-CA-CA-CD	2	4.20	180.0
CA-CA-CA-NC2	2	3.50	180.0
CT3-CA-CA-CA	2	3.10	180.0
CA-OS-CA-CA	2	4.00	180.0
CA-CA-CT3-HA	6	0.00	0.0
CA-CA-CD-OB	2	1.00	180.0
CA-CA-CD-OS	2	1.00	180.0
CA-CA-NC2-HC	2	2.50	180.0
CT2-NC2-CA-CA	2	0.00	140.0
NC2-CA-CA-CT2	2	1.10	180.0
NC2-CA-CA-CT3	2	1.10	180.0
NC2-CA-CA-HP	2	4.20	180.0
OS-CA-CA-HP	2	1.30	180.0
HP-CA-CA-HP	2	2.40	180.0
HP-CA-CA-CD	2	3.20	180.0
HP-CA-CA-CT3	2	4.20	180.0
CA-CD-OS-CT2	1	2.50	0.0
CA-NC2-CT2-CT3	2	1.00	-160.0
CA-NC2-CT2-HA	6	0.00	180.0
HC-NC2-CT2-HA	6	0.00	180.0
HC-NC2-CT2-CT3	3	0.00	180.0
NC2-CT2-CT3-HA	3	0.16	0.0
CD-OS-CT2-CT3	3	0.00	180.0
CD-OS-CT2-HA	3	0.00	180.0
CT2-OS-CD-OB	2	2.05	180.0
HA-CT3-CT2-OS	3	0.16	0.0
CT3-CT2-NC2-HC	3	0.00	180.0
HA-CT3-CT2-HA	3	0.16	0.0

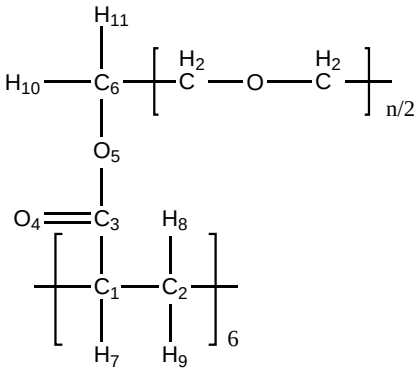

Figure 3.6: Atom numbering for cross-linker

Table 3.17: Atom numbering for the cross-linker.

Number	Atom type	Charge	Number	Atom type	Charge
C1	CT1R	-0.09	O5	OSR	-0.34
C2	CT2R	-0.18	C6	CT2R	-0.05
C3	CDR	0.73	H7-H11	HAR	0.09
O4	OBR	-0.52			

3.2.7 Force field parameters for cross-linker and ions

For consistency with the rhodamine molecule, the force field parameters for the acrylate cross-linker, chloride and sodium ions are from the CHARMM27 force field [61] and summarized in Table 3.17, 3.18, 3.19, 3.20, 3.21 and 3.22.

3.2.8 Cross-interaction terms and validation

For cross LJ interaction parameters between rhodamine and water, we used Lorentz-Berthelot combination rules and validated by calculating the diffusion coefficient of rhodamine in bulk water. We obtained a diffusion coefficient of 0.4243 $\times$ 10^{-5} cm^2/s which is within the range of values obtained in various experiments (0.3 $\times$ 10^{-5} cm^2/s to 0.5 $\times$ 10^{-5} cm^2/s)[72, 73, 74]. For cross LJ interaction parameters between ions and water, and between PEG chain and CHARMM atoms, we followed Patra et al. [75] and Zheng et al. [76] respectively and used Lorentz-Berthelot combination rules.

Table 3.18: Harmonic bond stretching parameters for the cross-linker.

Atom types	$k_{ij}^b(kcal/mol/\mathring{A}^2)$	$b_{ij}(\mathring{A})$
CT1R-CT2R	222.5	1.538
CT1R-CDR	200.0	1.522
CT1R-HAR	309.0	1.111

Table 3.19: Harmonic angle bending parameters for the cross-linker.

Atom types	$k^{\theta}_{ijk}(kcal/mol/rad^2)$	$\theta^0_{ijk}(^\circ)$
CT2-CT1-CD	52.00	108.0

Table 3.20: Urey-Bradley angle bending parameters for the cross-linker.

Atom types	$k^{\theta}_{ijk}(kcal/mol/rad^2)$	$\theta^0_{ijk}(^\circ)$	$k^b_{ij}(kcal/mol/\mathring{A}^2)$	$b_{ij}(\mathring{A})$
CT1-CT2-CT1	58.35	113.5	11.16	2.561
CT2-CT1-CT2	53.35	114.0	8.00	2.561
CT1-CD-OS	55.00	109.0	20.00	2.326
CT1-CD-OB	70.00	125.0	20.00	2.442
CT1-CT2-HA	33.43	110.1	22.53	2.179
CT2-CT1-HA	34.50	110.1	22.53	2.179
CD-CT1-HA	33.00	109.5	30.00	2.163

Table 3.21: The periodic dihedral function parameters for the cross-linker.

Atom types	n	$k_{\phi}(kcal/mol)$	$\phi_s(^\circ)$
CT1-CT2-CT1-HA	3	0.20	0.0
CT1-CT2-CT1-CT2	3	0.20	0.0
CT1-CT2-CT1-CD	3	0.20	0.0
CT1-CD-OS-CT2	2	2.05	180.0
CT2-CT1-CT2-HA	3	0.20	0.0
CT2-CT1-CD-OB	6	0.00	180.0
CT2-CT1-CD-OS	6	0.00	180.0
CD-CT1-CT2-HA	3	0.20	0.0
HA-CT1-CT2-HA	3	0.20	0.0
HA-CT1-CD-OB	6	0.00	180.0
HA-CT1-CD-OS	6	0.00	180.0

Table 3.22: Lennard-Jones parameters for the the ion molecules.

Atom types	$\epsilon(kcal/mol)$	$\sigma(\mathring{A})$
CL-CL	0.1501	4.0447
NA-NA	0.1000	2.5830

3.3 Simulation details

3.3.1 Simulation parameters

MD simulations were performed with gromacs 3.3.1[77]. Time integration was performed using the leap-frog algorithm with a time step of 1.0 fs. The short-range vdW interactions were computed using a cut-off scheme (cutoff distance, 1.0 nm). The long-range electrostatic interactions were computed by using a particle mesh Ewald method [77] (real space cutoff, 1.0 nm; FFT grid spacing, 0.12 nm, fourth-order interpolation). The Nosè-Hoover thermostat [45, 46] with a time constant of 0.5 ps was used to maintain the temperature at 300K.

3.3.2 System equilibration and data collection

We built the polymer network with all PEG chain segments in an all-trans conformation first and then inserted water molecules according to equilibrated water content in the hydrogel. After that, we let the system equilibrate for 1 ns in an NPT ensemble by maintaining a pressure of 1 bar (compressibility time constant of 0.2 ps; compressibility of 4.5×10^{-5} bar^{-1}) with a Parrrinello-Rahman barostat [78]. The energy, temperature and box size of the simulation box reached constant values during this equilibration process. Then we further equilibrated the system for additional 1 ns of simulation time using an NVT ensemble at 300 K. The energy and temperature of the simulation box reached constant values during this equilibration process. The resulting configuration is used as the starting point for further simulations. For collecting sufficient statistics to compute various properties, the simulations were run for 54 ns.

Chapter 4

Water structure and hydrogen bonding in hydrogel

4.1 Radial distribution function between polymer and water

The radial distribution function (RDF) $g(r)$ gives the probability density of finding a particle at a distance r from a given particle position. Because the PEG molecules are somewhat immobilized by cross-linkers as compared to the solvent, the water molecules that are close to PEG are expected to have much slower translational and rotational dynamics than water far away from PEG, similar to the behavior observed in confining environments [79, 80] and around biomacromolecules such as proteins [81, 82, 83] and DNA [84, 85, 86]. From an inspection of the radial distribution function between polymer ether oxygen and water oxygen, as shown in Figure 4.1, the perturbation of the water distribution around PEG ether groups, relative to the average water density, extended to a radius of about 1.04 nm from the polymer ether oxygen. The water around a PEG ether oxygen is less structured than water around a bulk water molecule. The RDFs here are similar to the RDFs between water and polymer oxygens for polymer-water solutions (PEO530 and 1,2-Dimethoxyethane) with 17% polymer weight percentage [87]. For different cross-linking densities, the peak positions of the RDFs between polymer ether oxygen and water oxygen are essentially the same (see Figure 4.1). As cross-linking density increases, the value of the first peak increases slightly (see Figure 4.1 inset).

The number of water oxygens per PEG ether oxygen, or the average coordination number, n_{OP-OW}, can be evaluated by the following equation:

$$n_{OP-OW} = \frac{N_{OW}}{V_{box}} \int_0^{R_{min}} 4\pi r^2 g_{OP-OW}(r) dr \tag{4.1}$$

where N_{OW} is the total number of water oxygens in the box, V_{box} is the volume of the box and R_{min} is the position of the first valley. The average coordination number is summarized in Table 4.1. The coordination number decreases as the cross-linking density increases. This implies that fewer water molecules come close to the polymer when cross-linking density increases and water content decreases. The variation of coordination

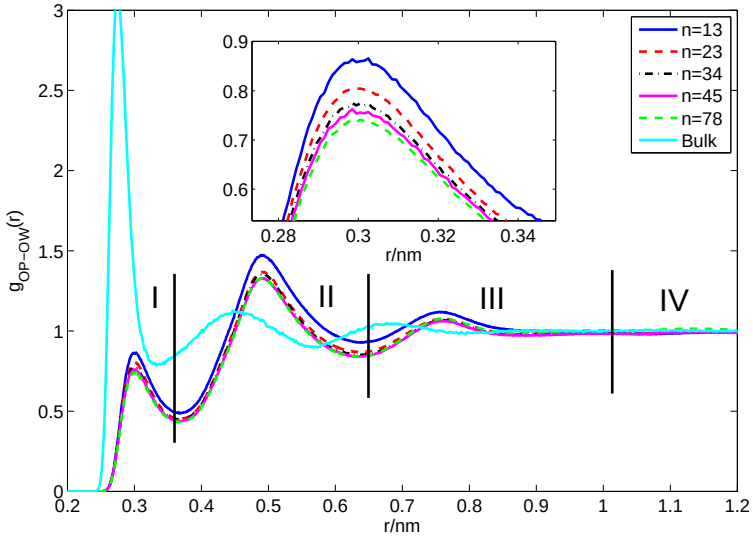

Figure 4.1: Radial distribution function (RDF) between oxygens of polymer ether and oxygen of water and between water oxygens in bulk water. Inset: amplification of the first peak. The RDF, $g_{OP-OW}(r)$, can be computed by normalizing the local density of water molecules at a distance of r from the polymer ether oxygens with the average density of water molecules in the total system. Water is divided into regions I, II, III and IV according to the distance from the polymer.

Table 4.1: Average coordination number for different cross-linking densities.

pre-polymer	n=13	n=23	n=34	n=45	n=78
	0.6792	1.0118	1.0382	1.4894	1.5985

number shown here is similar to the phenomenon observed in 1,2-Dimethoxyethane/water solutions with varying polymer concentration [69].

The water molecules in the gel system can be assigned into different regions according to their distance from the polymer ether oxygen atoms. We sampled the solvent in different regions, according to the $g_{OP-OW}(r)$ behavior [10]. Since there are three peaks in the curve, we divided the water into four regions. Region I ($r < 0.36$ nm) and region II (0.36 nm $< r <$ 0.64 nm) are considered as "close contact" regions. Water at distances between 0.64 nm and 1.04 nm, where the perturbation in the $g_{OP-OW}(r)$ was minor, is chosen as region III. The remaining water molecules are considered to be region IV. Water molecules in regions I-IV are characterized in terms of hydrogen bonding, relaxation times and diffusion coefficients.

Table 4.2: The average number of hydrogen bonds per water molecule in each region for different cross-linking densities. The last column shows water-water hydrogen bonding in region I, not including polymer-water hydrogen bonding. Regions II, III, and IV do not have any polymer-water HB. For region IV, at the highest cross-linking density n=13, there is no bulk region IV.

pre-polymer	I(total)	II	III	IV	I (water-water)
n=13	3.29	3.51	3.57	–	2.90
n=23	3.34	3.55	3.58	3.58	2.94
n=34	3.35	3.55	3.58	3.58	2.95
n=45	3.38	3.56	3.59	3.59	2.98
n=78	3.40	3.57	3.59	3.59	3.00

Table 4.3: Number of hydrogen bonds per polymer ether oxygen for different cross-linking densities in region I.

pre-polymer	n=13	n=23	n=34	n=45	n=78
	0.716	0.721	0.716	0.721	0.719

4.2 Water hydrogen bonding structure

The hydrogen bonding structure between water molecules and that between PEG ether oxygen and water was studied by analyzing the trajectory. Hydrogen bonding is defined by adopting the geometric criteria where the acceptor-donor (O $\cdots$ O) distance is less than 0.35 nm and the angle (O-H $\cdots$ O) is less than 30^o. For each cross-linking density, across different regions, the total number of hydrogen bonds is fairly constant except for a small dip in region I, as shown in Table 4.2.

In region I, the water-water hydrogen bonding is lowered, but that is made up for to some extent by the hydrogen bonding with the polymer ether oxygen which acts as an acceptor (see Table 4.3). The variation of the number of hydrogen bonds across different regions is similar to that seen in simulations of PVA hydrogels [10]. As cross-linking density increases, HB per water molecule decreases for all regions. For the highest cross-linking density case (n=13), there is no bulk region and region IV is undefined.

4.3 Hydrogen bond dynamics

The intermittent time autocorrelation function $c(t)$ expresses the probability that a randomly chosen pair of molecules is bonded at time t, provided that a bond existed at time $t = 0$, regardless of whether it was bonded in the interim time. $c(t)$ provides valuable insight into the relaxation of the system's H-bonding network. $c(t)$ is given by

$$c(t) = \frac{\langle h(t)h(0)\rangle}{\langle h(0)h(0)\rangle} \tag{4.2}$$

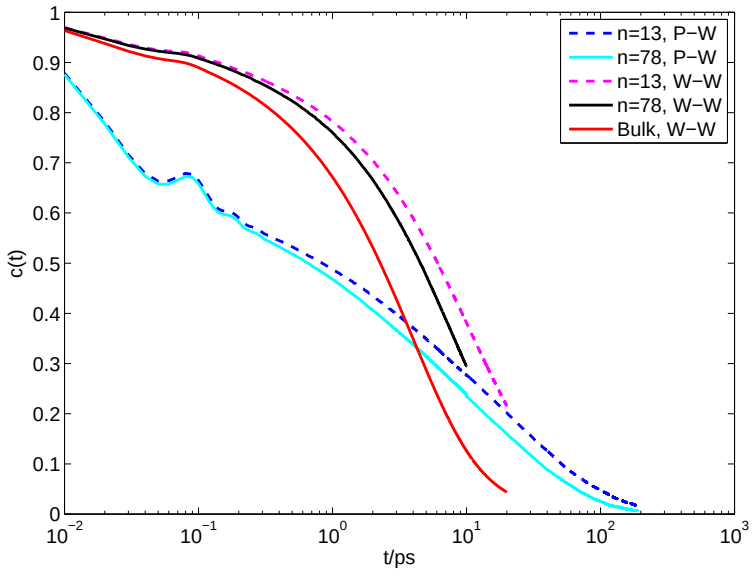

Figure 4.2: Decay of autocorrelation function $c(t)$ for polymer-water (P-W) and water-water (W-W) hydrogen bonding in region I. The autocorrelation function for the lowest (n=78) and the highest (n=13) cross-linking density cases are shown.

where $h(t)$ is 1 if molecules are bonded at time t and 0 if not. $\langle\rangle$ denotes average over all pairs of HB at $t = 0$ and over many time steps. Figure 4.2 shows the hydrogen bond autocorrelation functions for various cross-linking densities and bulk water. The decay can be divided into two parts: short time relaxations within the librational regime (< 0.1 ps) and long time relaxations beyond 0.1 ps. Water-water hydrogen bonding in the gel for $n = 78$ decays slower than the decay of water-water hydrogen bonding in the bulk. At the highest cross-linking density considered ($n = 13$), the decay is even slower. Compared to the water-water hydrogen bonding in the gel, the decay of the polymer-water hydrogen bonding shows different characteristics: polymer-water hydrogen bonds decay faster in the short time and is slower in the long time regime.

The long-time hydrogen bond dynamics is not characterized by an exponential relaxation with a single relaxation time τ_R [88], but by a stretched exponential function with a stretch parameter β as well [89]:

$$c(t) \approx A_0 exp[-(t/\tau_R)^{\beta}] \tag{4.3}$$

Stretched exponential function fit is considered to be purely empirical in most cases, but some physical significance may be attached to it for water. For bulk water, at room temperature, the physical origin of this stretched exponential at long times can be understood in terms of the coupling of hydrogen bond dynamics

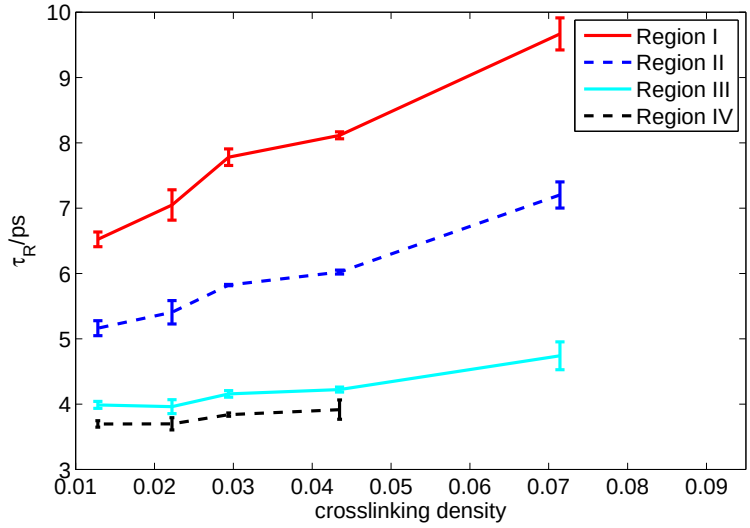

Figure 4.3: The relaxation time τ_R from the stretched exponential fit of the water-water HB autocorrelation function in regions I, II, III and IV.

.

to diffusion [90]. In our cross-linked PEGDA systems, we found that the stretched exponential parameters $\beta \approx 0.64$ and $A_0 \approx 1.0$ were almost independent of the cross-linking density. From the relaxation times τ_R calculated for different cross-linking densities (see Figure 4.3), it is evident that hydrogen bonds between water molecules survive longer when water is close to the polymer, similar to the observations in PVA hydrogels [10]. With increasing cross-linking density, the relaxation times of the hydrogen bonds increase as well. The results of the hydrogen bonding dynamics indicate that the existence of polymer leads to an overall slowing down of the system dynamics, and this slow-down is more severe as the cross-linking density increases.

To quantify the slowdown, we calculate the water diffusion coefficients in different regions for different cross-linking densities in the next chapter.

Chapter 5

Diffusion of molecules in hydrogel

5.1 Diffusion of water in hydrogels

5.1.1 Residence time of water

For water, to evaluate the limiting slope, we considered a time window equal to the average lifetime of the hydrogen bonds(HB) between PEG ether groups and water. The time evolution of this interaction is shown in Figure 4.2, where the time autocorrelation function of the hydrogen bonds, $c(t)$ is reported. The correlation time, t^*, was obtained by integrating polymer-water $c(t)$. t^* could be considered as the highest limiting value for the residence time in a particular region of a water molecule. The computed value of t^* varied between 10 to 20 ps depending on the cross-linking density.

5.1.2 Diffusion coefficient of water

The results of the diffusion coefficient for each region are summarized in Figure 5.1. The error bar in the plot is the standard deviation of the diffusion coefficients based on 3 trajectories for the same system with different initial configuration. The average water diffusion decreases as the cross-linking density increases, similar to the observations in poly (N-isopropylacrylamide) hydrogel [13] and in poly (methacrylic acid) hydrogel [91]. For each cross-linking density, water diffusion coefficient decreases as it approaches the polymer-water interface. The variation of the diffusion coefficient of water with cross-linking density is similar to the variation of the equilibrium water content shown in Figure 3.2.

5.2 Diffusion of ions in hydrogels

The diffusion coefficients of ions as a function of cross-linking density are shown in Figure 5.2(b) and Figure 5.2(c). For an ion concentration of 0.5 M, we observe that the diffusion of ions decreases as cross-linking density increases. Similar to the water case, ion diffusion also follows the water content variation with cross-linking density. Lobo et al. [92] studied diffusion of potassium chloride and lithium chloride in acrylamide

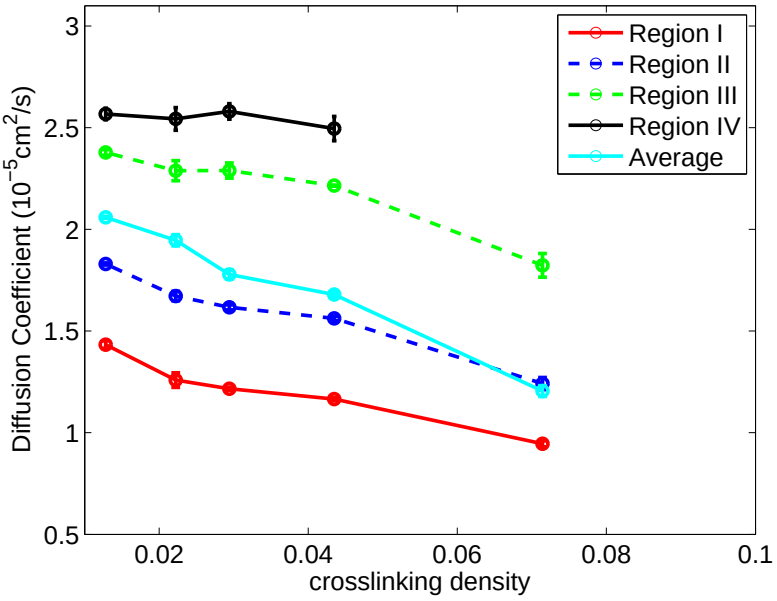

Figure 5.1: Diffusion of water in different regions as a function of the cross-linking density of the gel.

hydrogels and found that electrolyte diffusion depends on water content inside the polymer matrix. The results of our ion diffusion are comparable with experimental results for potassium chloride (KCl) and lithium chloride (LiCl) diffusion in hydrogels — for 1% cross-linking density acrylamide hydrogel with the same ion concentration, diffusion coefficients of KCl and LiCl within the gel are 31.9% and 42.7% of their values in aqueous solution.

5.3 Diffusion of rhodamine in hydrogels

To calculate the translational diffusion coefficient of rhodamine, we first estimated the rotational relaxation time of rhodamine. Rotational relaxation time is obtained from the relaxation time of the autocorrelation function $\langle \mathbf{n}(t) \cdot \mathbf{n}(0) \rangle$, where $\mathbf{n}(t)$ is the vector normal to the xanthylium plane of the rhodamine molecule. The computed rotational relaxation time of around 200 ps is comparable to the 100-200 ps in experiments [93]. A time window of 400 ps, a much larger value than the rotational relaxation time was used to compute the slope of the mean square displacement. Diffusion of rhodamine decreases with increasing cross-linking density, which is similar to the trend observed for water and ions, as shown in Figure 5.2(d). To accurately compute the diffusion coefficient with a linear MSD plot, 54 ns of simulation time was required. The diffusion coefficient of rhodamine in bulk water was 0.4243×10^{-5} cm^2/s. For the highest cross-linking density considered rhodamine diffusion is less than 5% of the bulk value.

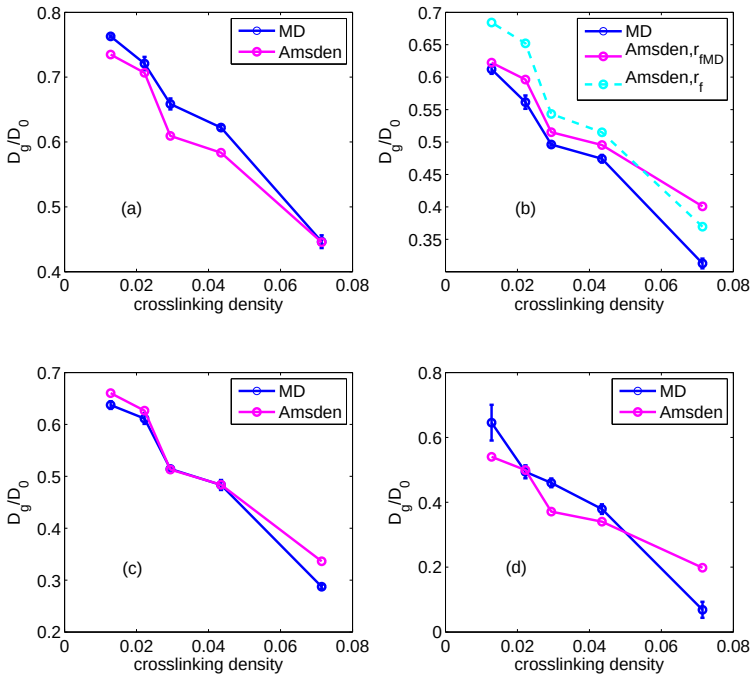

Figure 5.2: Normalized diffusion of water, ions and rhodamine as a function of cross-linking density obtained using molecular dynamics and theoretical prediction. The diffusion coefficient D_g is normalized with respect to the diffusion coefficient in bulk water D_0. Diffusion of (a) water (b) chloride ion (c) sodium ion and (d) rhodamine. For chloride ion, polymer fiber radius based on MD radial distribution function, r_{fMD}=0.5535 nm, is used, instead of r_f calculated from equation (5.2).

Our results are comparable to the diffusion of molecules of similar size in PEGDA gels in literature. Jang et al. [35] built PEG(1300)DA hydrogel system and studied diffusion of two small solute molecules – D-glucose and ascorbic acid (vitamin C). The diffusion coefficient of D-glucose in the gel was reported as $0.173 \pm 0.050 \times 10^{-5}\ cm^2/s$, which is one third of the D-glucose diffusion in water($0.6 - 0.7 \times 10^{-5}\ cm^2/s$) [94, 95, 96]. D-glucose has a hydrodynamic radius of $3.61 - 3.8$ Å[97, 98], that is comparable to 0.53 ± 0.03 nm of rhodamine 6G [99]. Using fluorescence correlation spectroscopy, Watkins et al. [15] studied diffusion of fluorescent probes Cl-NERF and Texas Red sulfonyl chloride, which have a hydrodynamic radius of 0.7 nm, in PEG(700)DA and PEG(1000)DA hydrogel. They obtained diffusion coefficients on the order of 10^{-8} cm^2/s.

5.4 Comparison with theory

5.4.1 Amsden's obstruction scaling theory

Over the years, many physical models have been developed to model the diffusion of small solutes in hydrogels[18, 19]. Solute behavior in hydrogels has been explained in terms of reduction in hydrogel free volume [20, 21, 22], enhanced hydrodynamic drag on the solute [23, 24], increased path length due to obstruction [25, 26], and a combination of hydrodynamic drag and obstruction effects [27].

Amsden [18] compares several theories and models for solute diffusion within hydrogels and suggests Amsden's theory where hydrodynamic models are combined with obstruction models as one of the best theories that matched several experimental results. According to the obstruction scaling theory [100, 101], the diffusion as a function of the polymer volume fraction is:

$$\frac{D_g}{D_0} = exp\left[-\pi\left(\frac{r_s + r_f}{k_s a \phi^{-0.75} C_\infty^{-0.25}(1-2\chi)^{-0.25} + 2r_f}\right)^2\right] \tag{5.1}$$

where a is the equivalent bond length of the monomer, ϕ is the polymer volume fraction, r_s is the radius of solute, r_f is the radius of polymer chain, C_∞ is the characteristic ratio of polymer, χ is the Flory-Huggins polymer/solvent interaction parameter, D_g is the diffusion coefficient of solute in gel, and D_0 is the diffusion coefficient of solute in water calculated from MD simulation and verified by literature [38, 102, 72, 73, 74]. Since the fitting parameter $k_s \simeq 1$ for the different polymers and solutes considered, Amsden proposed this model as a "universal" model for solute diffusion in hydrogels. The radius of the polymer chain is given by [100]:

$$r_f = \left(\frac{M_m v}{l \pi N_A}\right)^{1/2} \tag{5.2}$$

Table 5.1: Physical properties of the hydrogel used in Amsden's obstruction scaling theory.

$M_m(g/mol)$	$v(cm^3/g)$	$l(nm)$	$a(nm)$	$r_f(nm)$	C_∞	χ
44	0.8453[52]	0.36	1.54	0.2337	5.2[100]	0.46[100]

Table 5.2: Hydrodynamic radii and modified hydrodynamic radii used in this work for water, ions and rhodamine.

solute	water	chloride ion	sodium ion	rhodamine
bulk diffusion coefficient/$\times 10^{-5} cm^2/s$	2.70 [38]	1.85 [102]	1.32 [102]	0.4243 [72, 73, 74]
hydrodynamic radius (nm)	0.0914	0.1335	0.1870	0.5819
radius used in this work (nm)	0.276	0.332	0.358	0.4873

where l is the length of the monomer unit, M_m is the molecular weight of the monomer, v is the specific volume of the polymer, and N_A is the Avogadro number. The solute size r_s is the hydrodynamic radius of the solute computed by the Stokes-Einstein relation [100]:

$$r_s = \frac{k_B T}{f \pi \eta D_0} \tag{5.3}$$

where k_B is Boltzmann's constant, η is the viscosity of water at temperature T, and f is 4 for solutes whose size approaches that of the solvent (i.e. water) and 6 for solutes greater in size than the solvent [103].

5.4.2 Comparison between MD results and Amsden's theory

We compared our molecular dynamics simulation results with that from Amsden's obstruction scaling theory. The parameters used in equation (5.1) are listed in Table 5.1. According to Koneshan et al. [104] and Valente et al. [105], Stokes' law breaks down for small ions in highly polar solvents. Nightingale [106] extended the empirical correction to Stoke's law to provide a set of modified hydrodynamic radii for small ions. In using Amsden's theory, we used the modified hydrodynamic radii from Nightingale [106] for water, sodium and chloride ions rather than using the Stokes-Einstein relation. For rhodamine, we followed the same procedure as Jang et al. [35] to compute the hydrodynamic radius:

$$\langle r_h \rangle^{-1} = \frac{1}{N^2} \sum_{j \neq i}^{N} \sum_{i=1}^{N} \left\langle \frac{1}{r_{ij}} \right\rangle \tag{5.4}$$

where N is the number of atoms in the rhodamine molecule and r_{ij} is the distance between two atom pairs. The solute size r_s we used for water, sodium ion, chloride ion and rhodamine are listed in Table 5.2. For comparison, the hydrodynamic radii from the Stokes-Einstein relation are also listed.

In Figure 5.2 we compare the results from our MD simulations with the prediction from Amsden's theory

for water and the different solutes we considered. Diffusion data for water and sodium ion match better than that of chloride ion. The difference could be from the fact that the equation for calculating the radius of the polymer fiber, equation (5.2) does not take the ion size differences, and the different distances of closest approach into account. For the sodium ion, the first peak from the radial distribution function between oxygen of the polymer and the sodium ion was close to the value obtained from equation (5.2), but for the chloride ion, the first peak was at 0.5535 nm. Therefore we used 0.5535 nm as r_f for chloride ion.

Even though there is no perfect match, the theory matches reasonably well with MD results. As mentioned previously, the shapes of all the diffusion data are similar, and they follow the shape of the equilibrated water volume fraction, as shown in Figure 3.2. Unless the solute size and mesh size are comparable, such that the molecular level structure of the polymer network and the solute structure affect the diffusion, it is the equilibrated water content that is the key parameter in determining the diffusion coefficient. In experiments, factors such as concentration of pre-polymer solution, defects, rate of gelation etc., influence the final gel structure and thus the equilibrated water content and the diffusion data.

Chapter 6

Conclusions

To summarize, we have presented molecular dynamics investigations of diffusion of water and small solutes in PEGDA hydrogels of varying cross-linking densities. Diffusion coefficient of water and small solutes decreases as cross-linking density increases. Also the diffusion coefficients of water decrease when it comes closer to the polymer-water interface. The decrease in diffusion of water is correlated with the increase in hydrogen bonding relaxation times. The simulation results compare well with Amsden's obstruction scaling theory, if the hydrodynamic radii of the solutes can be computed more accurately than from the Stokes-Einstein relation. The diffusion behavior corresponds quite well with the equilibrated water content in each gel. This understanding of the diffusion of small molecules in hydrogel systems can be quite useful in applications including drug delivery systems, tissue engineering and contact lens.

References

[1] N. A. Peppas, Y. Huang, M. Torres-Lugo, J. H. Ward, and J. Zhang, "Physicochemical foundations and structural design of hydrogels in medicine and biology," *Annu. Rev. Biomed. Eng.*, vol. 2, no. 1, pp. 9–29, 2000. [Online]. Available: http://arjournals.annualreviews.org/doi/abs/10.1146/annurev.bioeng.2.1.9

[2] K. Lee and D. Mooney, "Hydrogels for tissue engineering." *Chem. Rev.*, vol. 101, no. 7, pp. 1869–79, 2001.

[3] M. Byrne, K. Park, and N. Peppas, "Molecular imprinting within hydrogels," *Adv. Drug Deliv. Rev.*, vol. 54, no. 1, pp. 149–161, 2002.

[4] R. Langer and N. Peppas, "Advances in biomaterials, drug delivery, and bionanotechnology," *AICHE J.*, vol. 49, no. 12, pp. 2990–3006, 2003.

[5] G. Underhill, A. Chen, D. Albrecht, and S. Bhatia, "Assessment of hepatocellular function within PEG hydrogels," *Biomaterials*, vol. 28, no. 2, pp. 256–270, 2007.

[6] F. Gabel, D. Bicout, U. Lehnert, M. Tehei, M. Weik, and G. Zaccai, "Protein dynamics studied by neutron scattering," *Q. Rev. Biophys.*, vol. 35, no. 04, pp. 327–367, 2003.

[7] R. Winter, "Synchrotron X-ray and neutron small-angle scattering of lyotropic lipid mesophases, model biomembranes and proteins in solution at high pressure," *BBA-Protein Struct. Mol. Enzymol.*, vol. 1595, no. 1-2, pp. 160–184, 2002.

[8] M. Koch, P. Vachette, and D. Svergun, "Small-angle scattering: a view on the properties, structures and structural changes of biological macromolecules in solution," *Q. Rev. Biophys.*, vol. 36, no. 02, pp. 147–227, 2003.

[9] G. Paradossi, F. Cavalieri, E. Chiessi, and M. Telling, "Supercooled Water in PVA Matrixes: I. An Incoherent Quasi-Elastic Neutron Scattering (QENS) Study," *J. Phys. Chem. B*, vol. 107, no. 33, pp. 8363–8371, 2003.

[10] E. Chiessi, F. Cavalieri, and G. Paradossi, "Water and Polymer Dynamics in Chemically Cross-Linked Hydrogels of Poly (vinyl alcohol): A Molecular Dynamics Simulation Study," *J. Phys. Chem. B*, vol. 111, no. 11, pp. 2820–2827, 2007.

[11] G. Cruise, D. Scharp, and J. Hubbell, "Characterization of permeability and network structure of interfacially photopolymerized poly (ethylene glycol) diacrylate hydrogels," *Biomaterials*, vol. 19, no. 14, pp. 1287–1294, 1998.

[12] H. Yasunaga, M. Kobayashi, S. Matsukawa, H. Kirosu, and I. Ando, "Structures and Dynamics of Polymer Gel Systems Viewed Using NMR Spectroscopy," *Annu. Rep. NMR Spectrosc.*, vol. 34, pp. 40–105, 1997.

[13] N. Tanaka, S. Matsukawa, H. Kurosu, and I. Ando, "A study on dynamics of water in crosslinked poly (N-isopropylacrylamide) gel by nmr spectroscopy," *Polymer*, vol. 39, pp. 4703–4706, 1998.

[14] J. Stringer and N. Peppas, "Diffusion of small molecular weight drugs in radiation-crosslinked poly (ethylene oxide) hydrogels," *J. Control. Release*, vol. 42, no. 2, pp. 195–202, 1996.

[15] A. Watkins and K. Anseth, "Investigation of molecular transport and distributions in poly (ethylene glycol) hydrogels with confocal laser scanning microscopy," *Macromolecules*, vol. 38, no. 4, pp. 1326–1334, 2005.

[16] R. Russell, A. Axel, K. Shields, and M. Pishko, "Mass transfer in rapidly photopolymerized poly (ethylene glycol) hydrogels used for chemical sensing," *Polymer*, vol. 42, no. 11, pp. 4893–4901, 2001.

[17] L. Weng, X. Zhou, X. Zhang, L. Zhang, and J. Xu, "Investigation into Molecular Diffusion in Hydrogels Using the Refractive Index Method," *Macromol. Rapid Commun.*, vol. 23, no. 16, pp. 968–971, 2002.

[18] B. Amsden, "Solute diffusion within hydrogels. Mechanisms and models," *Macromolecules*, vol. 31, no. 23, pp. 8382–8395, 1998.

[19] L. Masaro and X. Zhu, "Physical models of diffusion for polymer solutions, gels and solids," *Prog. Polym. Sci.*, vol. 24, no. 5, pp. 731–775, 1999.

[20] H. Yasuda, A. Peterlin, C. K. Colton, K. A. Smith, and E. W. Merrill, "Permeability of solutes through hydrated polymer membranes. Part III. Theoretical background for the selectivity of dialysis membranes," *Makromol. Chem.*, vol. 126, no. 1, pp. 177–186, 1969.

[21] N. Peppas and C. Reinhart, "Solute diffusion in swollen membranes. Part I. A new theory." *J. Membr. Sci.*, vol. 15, no. 3, pp. 275–287, 1983.

[22] S. Lustig and N. Peppas, "Solute diffusion in swollen membranes. IX: Scaling laws for solute diffusion in gels," *J. Appl. Polym. Sci.*, vol. 36, no. 4, pp. 735–747, 1988.

[23] R. Cukier, "Diffusion of Brownian spheres in semidilute polymer solutions," *Macromolecules*, vol. 17, no. 2, pp. 252–255, 1984.

[24] R. Phillips, W. Deen, and J. Brady, "Hindered transport of spherical macromolecules in fibrous membranes and gels," *AICHE J.*, vol. 35, no. 11, pp. 1761–1769, 1989.

[25] A. Ogston, "The spaces in a uniform random suspension of fibres," *Trans. Faraday Soc.*, vol. 54, pp. 1754–1757, 1958.

[26] L. Johansson, C. Elvingson, and J. Loefroth, "Diffusion and interaction in gels and solutions. 3. Theoretical results on the obstruction effect," *Macromolecules*, vol. 24, no. 22, pp. 6024–6029, 1991.

[27] E. Johnson, D. Berk, R. Jain, and W. Deen, "Hindered diffusion in agarose gels: test of effective medium model," *Biophysical J.*, vol. 70, no. 2, pp. 1017–1023, 1996.

[28] T. Hansson, C. Oostenbrink, and W. van Gunsteren, "Molecular dynamics simulations," *Curr. Opin. Struct. Biol.*, vol. 12, no. 2, pp. 190–196, 2002.

[29] A. Bizzarri and S. Cannistraro, "Molecular dynamics of water at the protein-solvent interface," *J. Phys. Chem. B*, vol. 106, no. 26, pp. 6617–6633, 2002.

[30] Y. Tamai, H. Tanaka, and K. Nakanishi, "Molecular Dynamics Study of Polymer-Water Interaction in Hydrogels. 1. Hydrogen-Bond Structure," *Macromolecules*, vol. 29, no. 21, pp. 6750–6760, 1996.

[31] Y. Tamai and H. Tanaka, "Dynamic properties of supercooled water in poly (vinyl alcohol) hydrogel," *Chem. Phys. Lett.*, vol. 285, no. 1-2, pp. 127–132, 1998.

[32] Y. Tamai and H. Tanaka, "Permeation of small penetrants in hydrogels," *Fluid Phase Equilib.*, vol. 144, no. 1-2, pp. 441–448, 1998.

[33] P. Netz and T. Dorfmuller, "Computer simulation studies on the polymer-induced modification of water properties in polyacrylamide hydrogels," *J. Phys. Chem. B*, vol. 102, p. 4875, 1998.

[34] J. Mijovic and H. Zhang, "Molecular dynamics simulation study of motions and interactions of water in a polymer network," *J. Phys. Chem. B*, vol. 108, no. 8, pp. 2557–2563, 2004.

[35] S. Jang, W. Goddard, and M. Kalani, "Mechanical and Transport Properties of the Poly (ethylene oxide)-Poly (acrylic acid) Double Network Hydrogel from Molecular Dynamic Simulations," *J. Phys. Chem. B*, vol. 111, no. 7, pp. 1729–1737, 2007.

[36] P. Gallo, M. Rovere, and E. Spohr, "Glass transition and layering effects in confined water: A computer simulation study," *J. Chem. Phys.*, vol. 113, p. 11324, 2000.

[37] G. Hummer, J. Rasaiah, and J. Noworyta, "Water conduction through the hydrophobic channel of a carbon nanotube," *Nature*, vol. 414, no. 6860, pp. 188–190, 2001.

[38] R. Mashl, S. Joseph, N. Aluru, and E. Jakobsson, "Anomalously immobilized water: a new water phase induced by confinement in nanotubes," *Nano Lett.*, vol. 3, no. 5, pp. 589–592, 2003.

[39] C. Won and N. Aluru, "Water Permeation through a Subnanometer Boron Nitride Nanotube," *J. Am. Chem. Soc.*, vol. 129, no. 10, pp. 2748–2748, 2007.

[40] P. Cicu, P. Demontis, S. Spanu, G. Suffritti, and A. Tilocca, "Electric-field-dependent empirical potentials for molecules and crystals: A first application to flexible water molecule adsorbed in zeolites," *J. Chem. Phys.*, vol. 112, p. 8267, 2000.

[41] Y. Fujiyoshi, K. Mitsuoka, B. de Groot, A. Philippsen, H. Grubmüller, P. Agre, and A. Engel, "Structure and Function of Water Channels," *Curr. Opin. Struct. Biol.*, vol. 12, no. 4, pp. 509–515, 2002.

[42] M. Sonoda and M. Skaf, "Carbohydrate Clustering in Aqueous Solutions and the Dynamics of Confined Water," *J. Phys. Chem. B*, vol. 111, no. 41, p. 11948, 2007.

[43] H. Lin, E. Van Wagner, B. Freeman, L. Toy, and R. Gupta, "Plasticization-Enhanced Hydrogen Purification Using Polymeric Membranes," *Science*, vol. 311, no. 5761, pp. 639–642, 2006.

[44] D. Frenkel and B. Smit, *Understanding molecular simulation: from algorithms to applications*. Academic Press, Inc. Orlando, FL, USA, 1996.

[45] S. Nosé, "A molecular dynamics method for simulations in the canonical ensemble," *Mol. Phys.*, vol. 100, no. 1, pp. 191–198, 2002.

[46] W. G. Hoover, "Canonical dynamics: Equilibrium phase-space distributions," *Phys. Rev. A*, vol. 31, no. 3, pp. 1695–1697, Mar 1985.

[47] T. Darden, D. York, and L. Pedersen, "Particle mesh ewald: An n? log (n) method for ewald sums in large systems," *J. Chem. Phys.*, vol. 98, p. 10089, 1993.

[48] U. Essmann, L. Perera, M. Berkowitz, T. Darden, H. Lee, and L. Pedersen, "A smooth particle mesh ewald method," *J. Chem. Phys.*, vol. 103, no. 19, pp. 8577–8593, 1995.

[49] B. Hess, H. Bekker, H. Berendsen, and J. Fraaije, "Lincs: a linear constraint solver for molecular simulations," *J. Comput. Chem.*, vol. 18, no. 12, pp. 1463–1472, 1997.

[50] N. Padmavathi and P. Chatterji, "Structural characteristics and swelling behavior of poly(ethylene glycol) diacrylate hydrogels," *Macromolecules*, vol. 29, no. 6, pp. 1976–1979, 1996.

[51] H. Ju, B. McCloskey, A. Sagle, Y. Wu, V. Kusuma, and B. Freeman, "Crosslinked poly (ethylene oxide) fouling resistant coating materials for oil/water separation," *J. Membr. Sci.*, vol. 307.

[52] H. Lin, T. Kai, B. Freeman, S. Kalakkunnath, and D. Kalika, "The effect of cross-linking on gas permeability in cross-linked poly (ethylene glycol diacrylate)," *Macromolecules*, vol. 38, no. 20, pp. 8381–8393, 2005.

[53] G. Tan, Y. Wang, J. Li, and S. Zhang, "Synthesis and Characterization of Injectable Photocrosslinking Poly (ethylene glycol) Diacrylate based Hydrogels," *Polym. Bull.*, vol. 61, no. 1, pp. 91–98, 2008.

[54] A. Datta, "Characterization of Polyethylene Glycol Hydrogels for Biomedical Applications," M.S. thesis, Louisana State University, 2007.

[55] P. Chuichay, E. Vladimirov, K. Siriwong, S. Hannongbua, and N. Rösch, "Molecular-dynamics simulations of pyronine 6G and rhodamine 6G dimers in aqueous solution," *J. Mol. Model.*, vol. 12, no. 6, pp. 885–896, 2006.

[56] W. Cornell, P. Cieplak, C. Bayly, I. Gould, K. Merz, D. Ferguson, D. Spellmeyer, T. Fox, J. Caldwell, and P. Kollman, "A second generation force field for the simulation of proteins, nucleic acids, and organic molecules," *J. Am. Chem. Soc.*, vol. 117, no. 19, pp. 5179–5197, 1995.

[57] J. Wang, P. Cieplak, and P. Kollman, "How well does a restrained electrostatic potential(resp) model perform in calculating conformational energies of organic and biological molecules?" *J. Comput. Chem.*, vol. 21, no. 12, pp. 1049–1074, 2000.

[58] P. Cieplak, J. Caldwell, and P. Kollman, "Molecular mechanical models for organic and biological systems going beyond the atom centered two body additive approximation: aqueous solution free energies of methanol and n-methyl acetamide, nucleic acid base, and amide hydrogen bonding and chloroform/water partition coefficients of the nucleic acid bases," *J. Comput. Chem.*, vol. 22, no. 10, pp. 1048–1057, 2001.

[59] H. Sun, "Compass: An ab initio force-field optimized for condensed-phase applications overview with details on alkane and benzene compounds," *J. Phys. Chem. B*, vol. 102, no. 38, pp. 7338–7364, 1998.

[60] W. Jorgensen, D. Maxwell, and J. Tirado-Rives, "Development and testing of the opls all-atom force field on conformational energetics and properties of organic liquids," *J. Am. Chem. Soc.*, vol. 118, no. 45, pp. 11 225–11 236, 1996.

[61] A. MacKerell Jr, N. Banavali, and N. Foloppe, "Development and current status of the charmm force field for nucleic acids," *Biopolymers*, vol. 56, no. 4, pp. 257–265, 2000.

[62] S. Mayo, B. Olafson, and W. Goddard, "Dreiding: A generic force field for molecular simulations," *J. Phys. Chem.*, vol. 94, no. 26, pp. 8897–8909, 1990.

[63] A. Rappe, C. Casewit, K. Colwell, W. Goddard III, and W. Skiff, "Uff, a full periodic table force field for molecular mechanics and molecular dynamics simulations," *J. Am. Chem. Soc.*, vol. 114, no. 25, pp. 10 024–10 035, 1992.

[64] W. Paul and G. Smith, "Structure and dynamics of amorphous polymers: computer simulations compared to experiment and theory," *Rep. Prog. Phys.*, vol. 67, no. 7, pp. 1117–1185, 2004.

[65] G. Smith, R. Jaffe, and D. Yoon, "Force field for simulations of 1, 2-dimethoxyethane and poly (oxyethylene) based upon ab initio electronic structure calculations on model molecules," *J. Phys. Chem.*, vol. 97, no. 49, pp. 12 752–12 759, 1993.

[66] R. Sorensen, W. Liau, L. Kesner, and R. Boyd, "Prediction of polymer crystal structures and properties: polyethylene and poly (oxymethylene)," *Macromolecules*, vol. 21, no. 1, pp. 200–208, 1988.

[67] H. Berendsen, J. Grigera, and T. Straatsma, "The missing term in effective pair potentials," *J. Phys. Chem.*, vol. 91, no. 24, pp. 6269–6271, 1987.

[68] D. Bedrov and G. Smith, "Molecular Dynamics Simulations of 1, 2-Dimethoxyethane in Aqueous Solution: Influence of the Water Potential," *J. Phys. Chem. B*, vol. 103, no. 18, pp. 3791–3796, 1999.

[69] D. Bedrov, O. Borodin, and G. Smith, "Molecular Dynamics Simulations of 1, 2-Dimethoxyethane/Water Solutions. 1. Conformational and Structural Properties," *J. Phys. Chem. B*, vol. 102, no. 29, pp. 5683–5690, 1998.

[70] D. Bedrov, O. Borodin, and G. Smith, "Molecular dynamics simulation of 1, 2-dimethoxyethane/water solutions. 2. dynamical properties," *J. Phys. Chem. B*, vol. 102, no. 47, pp. 9565–9570, 1998.

[71] A. Vaiana, A. Schulz, J. Wolfrum, M. Sauer, and J. Smith, "Molecular mechanics force field parameterization of the fluorescent probe rhodamine 6 G using automated frequency matching," *J. Comput. Chem.*, vol. 24, no. 5, pp. 632–639, 2003.

[72] J. Widengren, U. Mets, and R. Rigler, "Fluorescence correlation spectroscopy of triplet states in solution: a theoretical and experimental study," *J. Phys. Chem.*, vol. 99, no. 36, pp. 13 368–13 379, 1995.

[73] J. Schuster, F. Cichos, J. Wrachtrup, and C. von Borczyskowski, "Diffusion of Single Molecules Close to Interfaces," *Si. Mol.*, vol. 1, no. 4, pp. 299–305, 2000.

[74] M. Culbertson, J. Williams, W. Cheng, D. Stults, E. Wiebracht, J. Kasianowicz, and D. Burden, "Numerical Fluorescence Correlation Spectroscopy for the Analysis of Molecular Dynamics under Nonstandard Conditions," *Anal. Chem.*, vol. 79, no. 11, pp. 4031–4039, 2007.

[75] M. Patra and M. Karttunen, "Systematic comparison of force fields for microscopic simulations of NaCl in aqueous solutions: Diffusion, free energy of hydration, and structural properties," *J. Comput. Chem.*, vol. 25, no. 5, pp. 678–689, 2004.

[76] J. Zheng, L. Li, S. Chen, and S. Jiang, "Molecular Simulation Study of Water Interactions with Oligo (Ethylene Glycol)-Terminated Alkanethiol Self-Assembled Monolayers," *Langmuir*, vol. 20, no. 20, pp. 8931–8938, 2004.

[77] E. Lindahl, B. Hess, and D. van der Spoel, "GROMACS 3.0: a package for molecular simulation and trajectory analysis," *J. Mol. Model.*, vol. 7, no. 8, pp. 306–317, 2001.

[78] M. Parrinello and A. Rahman, "Polymorphic transitions in single crystals: A new molecular dynamics method," *J. Appl. Phys.*, vol. 52, no. 12, pp. 7182–7190, 1981. [Online]. Available: http://link.aip.org/link/?JAP/52/7182/1

[79] K. Bhattacharyya and B. Bagchi, "Slow dynamics of constrained water in complex geometries," *J. Phys. Chem. A*, vol. 104, no. 46, pp. 10 603–10 613, 2000.

[80] B. Bagchi, "Water dynamics in the hydration layer around proteins and micelles." *Chem. Rev.*, vol. 105, no. 9, pp. 3197–219, 2005.

[81] P. Fenimore, H. Frauenfelder, B. McMahon, and R. Young, "Bulk-solvent and hydration-shell fluctuations, similar to α-and β-fluctuations in glasses, control protein motions and functions," *Proc. Natl. Acad. Sci. U. S. A.*, vol. 101, no. 40, p. 14408, 2004.

[82] L. Nilsson and B. Halle, "Molecular origin of time-dependent fluorescence shifts in proteins," *Proc. Natl. Acad. Sci. U. S. A.*, vol. 102, no. 39, pp. 13 867–13 872, 2005.

[83] L. Hua, X. Huang, R. Zhou, and B. Berne, "Dynamics of Water Confined in the Interdomain Region of a Multidomain Protein," *J. Phys. Chem. B*, vol. 110, no. 8, pp. 3704–3711, 2006.

[84] S. Pal, L. Zhao, and A. Zewail, "Water at DNA surfaces: Ultrafast dynamics in minor groove recognition," *Proc. Natl. Acad. Sci. U. S. A.*, vol. 100, no. 14, p. 8113, 2003.

[85] S. Pal, P. Maiti, B. Bagchi, and J. Hynes, "Multiple Time Scales in Solvation Dynamics of DNA in Aqueous Solution: The Role of Water, Counterions, and Cross-Correlations," *J. Phys. Chem. B*, vol. 110, no. 51, pp. 26 396–26 402, 2006.

[86] D. Andreatta, J. Lustres, S. Kovalenko, N. Ernsting, C. Murphy, R. Coleman, and M. Berg, "Power-law solvation dynamics in DNA over six decades in time," *J. Am. Chem. Soc.*, vol. 127, no. 20, pp. 7270–7271, 2005.

[87] G. Smith and D. Bedrov, "A molecular dynamics simulation study of the influence of hydrogen-bonding and polar interactions on hydration and conformations of a poly (ethylene oxide) oligomer in dilute aqueous solution," *Macromolecules*, vol. 35, no. 14, pp. 5712–5719, 2002.

[88] A. Luzar and D. Chandler, "Effect of Environment on Hydrogen Bond Dynamics in Liquid Water," *Phys. Rev. Lett.*, vol. 76, no. 6, pp. 928–931, 1996.

[89] F. Starr, J. Nielsen, and H. Stanley, "Hydrogen-bond dynamics for the extended simple point-charge model of water," *Phys. Rev. E*, vol. 62, no. 1, pp. 579–587, 2000.

[90] A. Luzar and D. Chandler, "Hydrogen-bond kinetics in liquid water," *Nature*, vol. 379, no. 6560, pp. 55–57, 1996.

[91] H. Yasunaga and I. Ando, "Dynamic Behavior of Water in Hydro-swollen Crosslinked Polymer Gel as Studied by PGSE 1 H NMR and Pulse 1 H NMR," *Polym. Gels Networks*, vol. 1, pp. 83–92, 1993.

[92] V. Lobo, A. Valente, A. Polishchuk, and G. Geuskens, "Transport of non-associated electrolytes in acrylamide hydrogels," *J. Mol. Liq.*, vol. 94, no. 3, pp. 179–192, 2001.

[93] L. Deschenes and D. Bout, "Comparison of ensemble and single molecule approaches to probing polymer relaxation dynamics near T," *J. Chem. Phys.*, vol. 116, p. 5850, 2002.

[94] M. Marucci, S. Pettersson, G. Ragnarsson, and A. Axelsson, "Determination of a diffusion coefficient in a membrane by electronic speckle pattern interferometry: a new method and a temperature sensitivity study," *J. Phys. D-Appl. Phys.*, vol. 40, no. 9, pp. 2870–2880, 2007.

[95] M. Gagnon, P. Bissonnette, L. Deslandes, B. Wallendorff, and J. Lapointe, "Glucose Accumulation Can Account for the Initial Water Flux Triggered by Na+/Glucose Cotransport," *Biophys. J.*, vol. 86, no. 1, pp. 125–133, 2004.

[96] M. Andersson, A. Axelsson, and G. Zacchi, "Diffusion of glucose and insulin in a swelling N-isopropylacrylamide gel," *Int. J. Pharm.*, vol. 157, no. 2, pp. 199–208, 1997.

[97] B. Hannoun and G. Stephanopoulos, "Diffusion coefficients of glucose and ethanol in cell-free and cell-occupied calcium alginate membranes," *Biotechnol. Bioeng.*, vol. 28, pp. 829–835, 1986.

[98] S. Schultz and A. Solomon, "Determination of the Effective Hydrodynamic Radii of Small Molecules by Viscometry," *J. Gen. Physiol.*, vol. 44, no. 6, pp. 1189–1199, 1961.

[99] J. Karolin, C. Geddes, K. Wynne, and D. Birch, "Nanoparticle metrology in sol- gels using multiphoton excited fluorescence," *Meas. Sci. Technol.*, vol. 13, no. 1, pp. 21–7, 2002.

[100] B. Amsden, "An obstruction-scaling model for diffusion in homogeneous hydrogels," *Macromolecules*, vol. 32, no. 3, pp. 874–879, 1999.

[101] B. Amsden, "Modeling solute diffusion in aqueous polymer solutions," *Polymer*, vol. 43, no. 5, pp. 1623–1630, 2002.

[102] R. Mills and V. Lobo, *Self-diffusion in Electrolyte Solutions: A Critical Examination of Data Compiled from the Literature*. Elsevier Publishing Company, 1989.

[103] G. Flynn, S. Yalkowsky, and T. Roseman, "Mass transport phenomena and models: theoretical concepts." *J. Pharm. Sci.*, vol. 63, no. 4, pp. 479–510, 1974.

[104] S. Koneshan, R. Lynden-Bell, and J. Rasaiah, "Friction coefficients of ions in aqueous solution at 25 C," *J. Am. Chem. Soc.*, vol. 120, no. 46, pp. 12 041–12 050, 1998.

[105] A. Valente, A. Polishchuk, V. Lobo, and G. Geuskens, "Diffusion coefficients of lithium chloride and potassium chloride in hydrogel membranes derived from acrylamide," *Eur. Polym. J.*, vol. 38, no. 1, pp. 13–18, 2002.

[106] E. Nightingale Jr, "Phenomenological Theory of Ion Solvation. Effective Radii of Hydrated Ions," *J. Phys. Chem.*, vol. 63, no. 9, pp. 1381–1387, 1959.